https://doi.org/10.5194/egusphere-2025-4849
Preprint. Discussion started: 8 December 2025

Snow Mass Components Analysis: Greater Contribution to Atmospheric Water Vapor than to Water Resources on the Tibetan and Pamir Plateaus

Changlong Li[1,2], Lan Cuo[1,3,5], Yongxin Zhang[4], Xuefeng Zhang[1,5], Xuan Li[1,5], Mei Hou[6], Aihui Wang[7], Liqiao Liang[1,3]

[1]Institute of Tibetan Plateau Research, Chinese Academy of Sciences, Beijing, China
[2]China Earthquake Disaster Prevention Center, Beijing, China
[3]State Key Laboratory of Tibetan Plateau Earth System, Resources and Environment, Institute of Tibetan Plateau Research, Chinese Academy of Sciences, Beijing, China
[4]National Center for Atmospheric Research, Boulder, CO, USA
[5]University of Chinese Academy of Sciences, Beijing, China
[6]Suzhou University, Suzhou, Anhui, China
[7]Institute of Atmospheric Physics, Chinese Academy of Sciences, Beijing, China

Correspondence to: Lan Cuo (lancuo@itpcas.ac.cn) & Liqiao Liang (liangliqiao@itpcas.ac.cn)

Abstract. Snow in the high-altitude and high-latitude regions is essential for water resources and climate regulation. However, studies on snow mass balance components in alpine areas like the Tibetan and Pamir Plateaus (TPP) are limited. To fill the gap, a novel snow simulation framework was developed, combining in-situ snow depth, satellite snow cover, and point- and grid-scale modelling, supported by sensitivity analysis, automatic calibration, and deep learning. Key snow components—snowfall, snow water equivalent (SWE), refrozen snow, sublimation, evaporation, and snowmelt—were simulated across the TPP from 1962 to 2019 with reliable accuracy. Regionally averaged annual snowfall and refrozen snow—together representing snow pack input—were 70.67 ± 17.32 mm and 16.56 ± 3.85 mm, respectively. On average, 38% of this input is converted into SWE and snowmelt that contributes 12–19% of total river discharge over the TPP, while the remaining 62% is lost to the atmosphere through sublimation and evaporation. Snow contributes less to water resources than to atmospheric moisture over the TPP on annual average. Seasonal snow patterns vary by region: in the Pamirs snow accumulates throughout the winter, making March–April SWE a key water resource indicator; while in the Tibetan Plateau, limited snow accumulation means total annual snowmelt better representing snow water resources. Significant regional declines have been simulated for key snow

https://doi.org/10.5194/egusphere-2025-4849
Preprint. Discussion started: 8 December 2025

components though the trends vary spatially, potentially greatly influencing weather and climate both locally and remotely. Precipitation drives SWE changes in the north and west of the TPP, while temperature and wind speed play greater roles in the center and south.

1 Introduction

Snow is a vital component of the cryosphere, water cycle, climate system, and economy in the high-altitude and high-latitude (HAL) region. In the Northern Hemisphere, monthly snow cover spans from 3–47×10⁶ km², covering 2–36% of global land (Estilow et al., 2015). Snow water equivalent (SWE) and snowmelt are crucial water resources for water supply, hydropower, irrigation, navigation, and urban use (Barnett et al., 2005; Hamlet et al., 2005; Fang et al., 2022). Snow also contributes to atmospheric water vapor through sublimation and evaporation. In Asia, snowmelt from the Tibetan and Pamir Plateaus (TPP) contributes to streamflow in the headwaters of Asia's major rivers (Immerzeel et al., 2020; Cuo et al., 2014). TPP snow cover also influences weather and climate both locally and remotely (Turner et al., 2011). Additionally, snow-based sports and recreation, such as the Winter Olympics, are significant economic and social activities.

Significant progress has been made in studying snow in the past few decades around the globe (Chen et al., 2014; Li et al., 2023; Shao et al., 2022), leading to findings in snow metamorphism, phenology, cover, depth, snow mass balance, snow contribution to streamflow, as well as their responses to climate change (Hamlet et al., 2005; Pomeroy et al., 2000; King et al., 2001; Bowling et al., 2004; Qin et al., 2006; You et al., 2011; Li et al., 2018; Smith et al., 2018; Bormann et al., 2018; Kirkham et al., 2019; Kraaijenbrink et al., 2021; Chen et al., 2021; Jin et al., 2022; Gao et al., 2023; Liu et al., 2023b; Ma et al., 2023; Lundquist et al., 2024; Hou et al., 2025). Composed of air and three phases of water, snow has unique characters such as high albedo and emissivity, low thermal conductivity and roughness length, and temporally varied density. Due to high albedo and emissivity, snow reflects a great amount of incoming solar radiation back to the atmosphere while suppresses outgoing longwave radiation compared to non-snow surface, resulting in low surface temperature and reduced sensible heat flux between the atmosphere and snow surface (Groisman et al., 1994). Due to low thermal conductivity, relatively thick snow functions as an insulator and decouples soil from the atmosphere, resulting in

https://doi.org/10.5194/egusphere-2025-4849
Preprint. Discussion started: 8 December 2025

higher soil temperature than air temperature in snow season (Li et al., 2024). Snow phenology also dictates that high latent heat flux is produced at the expense of sensible heat flux during melting season. Reduced snow/ice due to global warming has exerted a positive albedo feedback effect that has resulted in the Arctic amplification (Screen et al., 2010; Cohen et al., 2020). The sensitivity of SWE to the changes of individual climate factors varies with climate regime, with relatively warm (cold) alpine regions being more (less) sensitive to temperature increase (Hamlet et al., 2005). This gives rises to strong reduction of SWE in sensitive regions, but small or little reduction or even increased SWE depending on precipitation changes in the other regions (Hamlet et al., 2005; Li et al., 2018). For the TPP, with its vast area and extensive snow cover but with diverse climates within the TPP, how snow mass balance components behave temporally and spatially responding to climate change has been less well studied and clearly warrants further investigation.

Snow mass balance components include snowfall (SF), refrozen snow (SRF), snowmelt (SM), standstill snowpack and blowing snow sublimation and evaporation, and SWE. SWE in late March or early April is usually used to represent snow water resource in a hydrological year over regions where winter snow accumulates. Among snow mass balance terms, only SWE is often measured, which is the case for the TPP as well.

Snow sublimation including standstill snowpack surface sublimation and blowing snow sublimation (BSS) occurs when snow directly transforms from solid to vapor. Evaporation could also occur from melt water in snowpack. Sublimation and evaporation directly contribute to atmospheric water vapor and are losses from the water resource perspective. Sublimation requires higher energy (2838 J/g at 0 °C and standard pressure) that can be obtained from local net radiation and wind advected energy, than that for snow evaporation (2501 J/g) and melt (334 J/g). Snow sublimation can happen under low air temperature, high vapor pressure deficit and windy weather conditions according to the bulk aerodynamic theory (King et al., 2001; Stigter et al., 2018). Standstill snowpack surface sublimation and evaporation (SSSS) can be directly obtained through a snow lysimeter and eddy covariance, and can also be calculated using vapor pressure, wind speed and radiation.

BSS is one of the most uncertain components in snow mass balance terms (Screen et al., 2010; González-Herrero, 2025). Blowing snow is composed of wind-driven suspended snow particles which

https://doi.org/10.5194/egusphere-2025-4849
Preprint. Discussion started: 8 December 2025

can be calculated and measured by blowing snow sensors. Probability of the occurrence of blowing snow can be represented by cumulative normal probability distribution that depends on snow age, wind speed, vegetation roughness and air temperature. The blowing snow process has already been incorporated into snow and land surface models (Pomeroy and Li, 2000; Bowling et al., 2004; Liston et al., 2007), some of which use Laplace distribution to represent the variation of wind speed in sub-grid cells. However, few large-scale models simulate blowing snow sublimation (Lundquist et al., 2024). Sublimation is one of the major sources of uncertainty in land surface models (Chen et al., 2014). Studies have shown that snow sublimation could remove 10-15% of precipitation in the Arctic (King et al., 2001), 21% of annual snowfall and 17% of SWE in Langtang basin in Nepalese Himalaya Mountains (Stigter et al., 2018; Saloranta et al., 2019), and 15-41% of annual snowfall in Canadian prairies (Pomeroy and Gray, 1995). Thus, any omission of snow sublimation in snow mass balance calculation over the HAL could severely underestimate snow losses while overestimate snowmelt contribution to water resources.

Snowmelt is an important contributor to soil moisture and streamflow in the HAL, and is another key source of uncertainty in land surface models (Chen et al., 2014) due to limited measurement and studies in tracking snowmelt contribution to streamflow (Liu et al., 2023b). Under warming climate, the general change patterns in nival or nival-pluvial mixed watersheds are advanced spring peak flow, reduced summer flow, increased evapotranspiration and reduced soil moisture which are also predicted to continue in the future in some cases due to advanced snowmelt season (Barnett et al., 2005; Qin et al., 2022). Such shifts in hydrological regime pose risks in water resources management and utilization in the HAL. Clearly, understanding snow mass components and their changes could contribute to the mitigation of such risks in alpine regions.

Despite advancement in snow physics and hydrological studies, snow measurement in alpine regions continuous to face challenges (Chen et al., 2014). In-situ measurements are mostly in low-elevation valleys and are unable to represent high-mountain snow conditions, while passive microwave remote sensing has difficulties in resolving snow depth and SWE in complex terrain (Dozier et al., 2016). This measurement gap limits our understanding of snow mass in the alpine where vast snow storage feeds

https://doi.org/10.5194/egusphere-2025-4849
Preprint. Discussion started: 8 December 2025

rivers, leading to high uncertainties in the quantification of global and regional snow water storage and water resources (Smith and Bookhagen, 2018; Pulliainen et al., 2020).

As Asia's water tower with the largest cryospheric components outside the poles, the alpine TPP faces even greater challenges in snow mass study due to not only scarce but also sometimes low-quality data. There are several studies on SWE, snowmelt and snow sublimation in the TPP (Gao et al., 2023; Stigter et al., 2018; Ueno et al., 2007; Zhang et al., 2013; Li et al., 2019; Sahadeep, 2019), but many of them suffer from either data quality issues or limited spatial or temporal coverage. Current Earth System Models significantly underestimate the number of freezing days while systematically overestimating SWE when simulating snow variability over the TPP (Chai et al., 2025). Bian et al. (2019) found that 14 SWE datasets from satellites, reanalysis, and modelling products captured SWE seasonal and interannual variations but overestimated SWE by an order of magnitude on the TPP. Li et al. (2023) reported poor snow depth representation in the Sentinel-1, ERA5-Land, ERA5, and MERRA-2 datasets. Some recent snow mass modelling studies on the TPP consider sublimation but these studies focus either on winter only (Zhang et al., 2015) or lack a blowing snow sublimation component (Yang et al., 2021; Yang et al., 2022). Additionally, global SWE products like GlobSnow (Bormann et al., 2018) and RRM SWE (Shao et al., 2022) exclude mountainous areas such as the TPP to avoid poor data quality. On the other hand, given the importance of mountain snow, the World Meteorological Organization (WMO) Global Cryosphere Watch has designated snow studies as a long-term priority (Smith and Bookhagen, 2018; Bormann et al., 2018; Kirkham et al., 2019; Pulliainen et al., 2020; Yang et al., 2021). Clearly, a novel and comprehensive analysis framework that combines modelling and measurement is needed to create reliable datasets for credible snow mass component studies over the entire TPP.

This study aims to develop such a framework through combining measurement and physically based hydrological models assisted with deep learning, and to use this framework to address the knowledge gap in snow mass components on the alpine TPP. Specifically, we strive to 1) produce high quality spatiotemporally continuous SWE datasets given that SWE is widely used to represent snow water resource; 2) investigate the spatiotemporal characteristics of snow mass balance components; 3) understand the importance of snow to water resources and atmosphere in the TPP; and 4) examine the

https://doi.org/10.5194/egusphere-2025-4849
Preprint. Discussion started: 8 December 2025

relationships between the changes in SWE and climate factors. The study will improve the understanding of snow mass components and snow water resources in Asian alpine regions.

2 Methodology

2.1 Study area

The TPP, located in 65°E−105°E and 27°N–40°N, is composed of the expansive Tibetan Plateau (TP) in the east and the smaller Pamir Plateau in the west (Fig. 1a). It has an average elevation and an area of about 4000 m and 3.13×10^6 km^2, respectively. Several massive mountain ranges such as the Himalayas, Gangdese, Nyenchen Tangla, Tanggula, East Kunluns and Qilian surround or transect the TPP from the south to the north. Large plains and valleys such as the Qiangtang, Hoh-xil and Qaidam lie between the mountain ranges. The Hindu Kush and Karakoram lie in the Pamirs from which the West Kunlun extends toward northeast and enters the Tibetan Plateau. In the southeast and northwest, the Hengduan Mountains and Altyn Mountains are situated, respectively. Numerous smaller mountains also spread in the interior TPP. These large and small mountains are the headwaters of major Asian rivers, including the Yellow, Yangtze, Mekong, Salween, Brahmaputra, Ganges, Indus, and Amu Darya. Based on seasonal precipitation distribution, basins on the TPP can be divided into westerly circulation dominated and monsoon dominated basins. Westerly dominated basins include Amu Darya and Indus where precipitation falls primarily during winter and spring; the rest are monsoon dominated basins where precipitation occurs mainly in May-October.

https://doi.org/10.5194/egusphere-2025-4849
Preprint. Discussion started: 8 December 2025

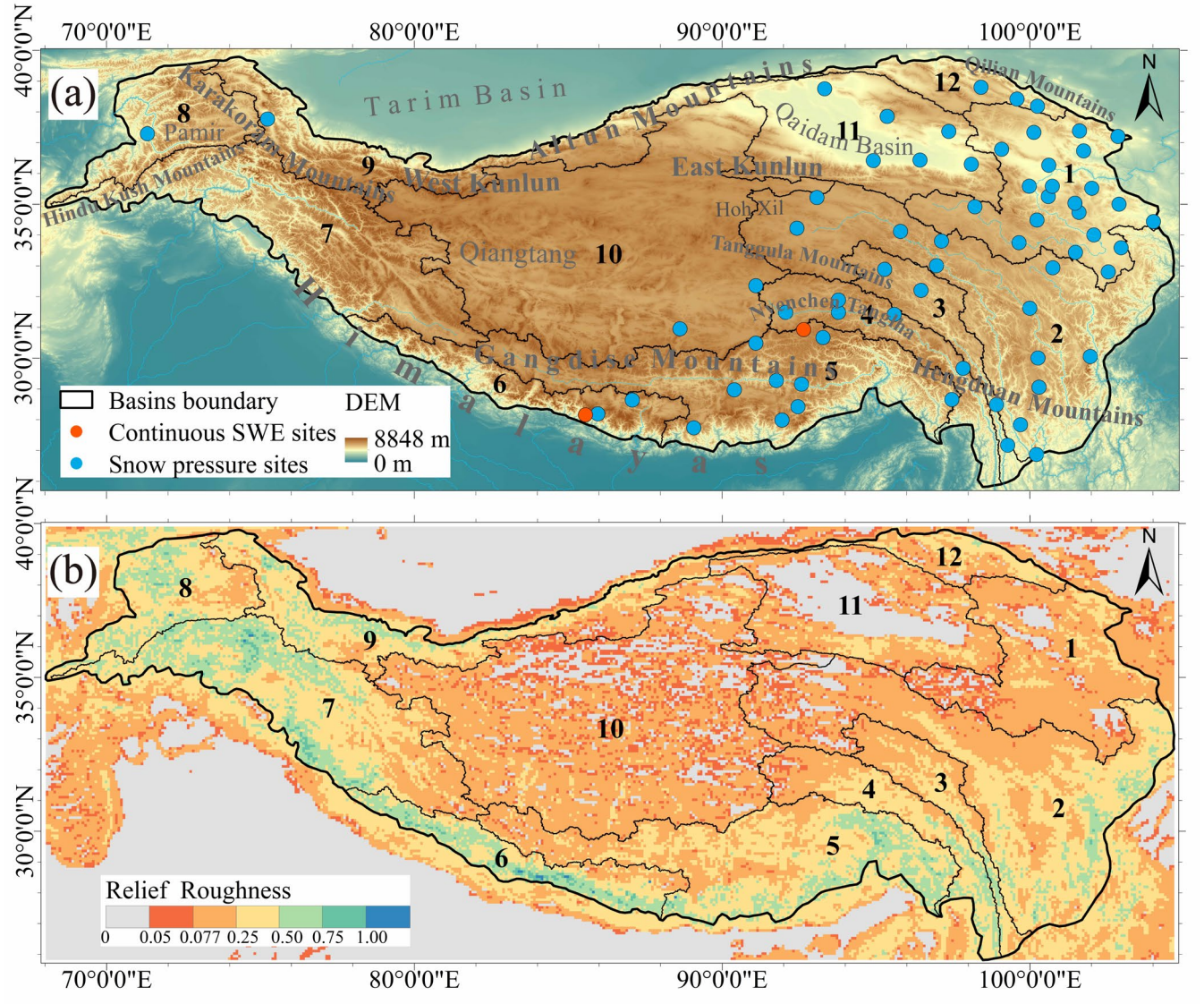

Figure 1: Study area. (a) elevation (m) and locations of the measurement sites, and (b) relief roughness at 30 arc sec resolution on the Tibetan and Pamirs Plateaus (TPP). In (a), the blue dots represent snow pressure measurement sites and the two red dots (Gangjiala station near the south boundary and Lindi station between Basins 5 and 4) denote continuous SWE measurement sites. Numerical numbers in both (a) and (b) represent river basins: 1) upper Yellow River, 2) upper Yangtze River, 3) upper Mekong River, 4) upper Salween River, 5) Brahmaputra, 6) upper Ganges River, 7) upper Indus River, 8) upper Amu Darya, 9) upper Tarim River, 10) Inner Tibetan Plateau, 11) Qaidam Basin, and 12) Qilian Mountain Basin.

Using 90-m and 1-km resolution elevation maps, we produced 1-km relief roughness map according to Körner et al. (2011) by first subtracting minimum elevation from maximum elevation in the 90-m cells enclosed within a 1-km grid cell and then dividing by half of the 1-km cell's resolution. The areas with

https://doi.org/10.5194/egusphere-2025-4849
Preprint. Discussion started: 8 December 2025

relief roughness greater than 0.077 account for more than 70% of the TPP (Fig. 1b), indicating that more than 70% of the domain is occupied by mountains based on the definition by Körner et al. (2011). The rugged terrain complicates both in-situ and remote sensing snow mass measurements, presenting challenges for snow mass studies and leading to a widely debated question: how much snow actually contributes to rivers on the TPP.

2.2 Data

Since we used both point- and grid-scale models and a deep learning method to model and study snow, data used include model forcings, spatial inputs, and measurements for evaluation. For the Variable Infiltration Capacity (VIC) hydrological model (Liang et al., 1994, 1996) running at grid scale covering the TPP, daily maximum and minimum air temperature, precipitation and wind speed in 0.25°×0.25° resolution during 1957-2020 were the forcings. This gridded dataset (LC forcing) was generated following Cuo et al. (2013a; 2017). In total, 966 precipitation, 466 maximum and 435 minimum air temperature, and 427 wind speed stations (Fig. S1, see Supplementary Material) from the China Meteorological Administration (CMA, https://data.cma.cn/) and NOAA-daily collection (https://www.ncei.noaa.gov) were used to create the gridded forcing data. In addition, 15 stations from other sources (see Table S1 in Supplementary Material) were used to independently evaluate the gridded forcing. The evaluation results presented in Table S2 show that air temperature has quite good correlation coefficients (CC) between observations and gridded values at cells that cover the stations; precipitation and wind speed also exhibit acceptable correlation (CC>0.4) at 10 (for precipitation) and 11 (for wind speed) stations indicating that the observed daily variations in meteorological forcings are satisfactorily represented by the gridded data. However, relative biases and RMSEs vary considerably from station to station due to the scale mismatch between a 0.25°×0.25° cell and the corresponding station, especially when terrain is complex.

Spatial inputs in the VIC include land cover, soil and elevation. For land cover maps, the European Space Agency CCI-LC (300-m, https://www.esa-landcover-cci.org/), GLASS-GLC (5-km, https://doi.pangaea.de/10.1594/PANGAEA.913496) and GLC_FCS30-2020 (30-m, https://data.casearth.cn) datasets were initially collected and evaluated using ground truths of land cover

https://doi.org/10.5194/egusphere-2025-4849
Preprint. Discussion started: 8 December 2025

types obtained during summer field trips and from previous studies (Tables S3, S4). CCI-LC 2020 land cover maps exhibit the best quality in resolving grassland, the dominant land cover type on the TPP. To represent land cover changes over a sequence of 10-year periods, CCI-LC in 1992, 2000, 2010 and 2020 were selected. CCI-LC does not provide land cover map prior to 1992. Areal fractions of all land cover types in each 0.25°×0.25° grid cell were calculated and used as model input. The VIC model was run for four continuous periods in consistence with the land cover maps: 1957-1992, 1993-2000, 2001-2010 and 2011-2020 using land cover 1992, 2000, 2010 and 2020, respectively. Model outputs were subsequently combined to form the full period (1957-2020) simulations. 1957-1961 was the model warming-up period, and 1962-2019 was the analysis period. Soil class and parameters were from the Harmonized World Soil Database (https://www.fao.org). Elevation was from the NASA SRTM (Shuttle Radar Topography Mission, https://srtm.csi.cgiar.org/srtmdata/). VIC simulated SWE was evaluated using station-based SWE.

For the VIC running at station scale, observed hourly precipitation, air temperature, wind speed, incoming shortwave and longwave radiation, air pressure and vapor pressure from the CMA were used to drive the model. Land cover, soil and elevation data for the station-scale VIC were from the same sources as described above. During snow season, precipitation undercatch affects snow simulation and needs to be corrected (Miao et al., 2024). The WMO recommended equations (Kochendorfer et al., 2022) and related wind speed calculated at various heights for Chinese stations (Zheng et al., 2018) were used to calculate catch efficiency (CE) following Eq. (1) and Eq. (2) for correcting precipitation undercatch at 66 SWE simulation stations:

$$CE = e^{-0.063\times 0.71127451\times \mathrm{U}(h)\times\left(1-\left[\tan^{-1}(1.22\times T_{air})+0.66\right]\right)} \quad (1)$$

$$\mathrm{U}(h) = \frac{[ln(h/z_0)]}{[ln(H/z_0)]}\times \mathrm{U}(H) \quad (2)$$

where $\mathrm{U}(h)$ is wind speed at precipitation gauge height h, Tair is air temperature at 2 m, H is anemometer height and its corresponding wind speed is $\mathrm{U}(h)$, z_0 is roughness length (0.01 in cold seasons and 0.03 in warm seasons). The corrected precipitation in the snow season increases noticeably

https://doi.org/10.5194/egusphere-2025-4849
Preprint. Discussion started: 8 December 2025

in the eastern TPP compared to the original values, more so in the southern and northeastern peripheries (Fig. S2).

On the TPP, only snow depth is measured routinely, and no other snow mass measurements are available. SWE is not directly measured at meteorological stations in China but is computed using snow depth and snow pressure measurements (see Supplementary Material). Such SWE is not temporally continuous. We collected about 400 stations from the CMA and Meteorological Agency in Tajikistan, and after quality control and observation period check, SWE at 66 stations in 1980-2009 was used. Temporally continuous SWE observations at Ganjia La (28.1545°N, 85.5625°E, 4962 m, gravel/rock) during 2016-2018 (Kirkham et al., 2019) and at Lindi village in the Tibetan Autonomous Region (30.9243°N, 92.6513°E, 4853 m, grass, our own observation site) during 2022 were also collected (Fig. 1a).

Two passive microwave remote sensing SWE datasets, 500-m resolution NASA-HMA (High Mountain Asia) product for June 2002 – September 2011 (https://www.sciengine.com/CSD/doi/10.11922/csdata.2018.0064.zh) and 25-km resolution FY3 (FengYun-3 satellite) product for January 2015 – November 2019 (http://www.nsmc.org.cn/) were also used for comparison and evaluation. These two SWE products were not evaluated by Bian et al. (2019).

To regionalize the calibrated and validated VIC sensitive snow parameters at 66 stations, spatially continuous MODIS 500-m resolution snow cover products, MOD09GA and MYD09GA (https://data.tpdc.ac.cn/en/) in 2000-2009, were used to train and evaluate a machine learning scheme. Snow on the glacier surface accumulates through the years and eventually becomes ice, thus snow in the 117 cells with glacier area greater than 60% of the cell area was not considered during the analysis. Glacier area was from the RGI 6.0 (Randolph Glacier Inventory, https://nsidc.org/data/nsidc-0770/versions/6).

https://doi.org/10.5194/egusphere-2025-4849
Preprint. Discussion started: 8 December 2025

2.3 Models

ΔSNOW model (Winkler et al., 2021), a free R package that semi-empirically calculates snow density at point scale, was used to reconstruct temporally continuous SWE at 66 SWE stations (Fig. 1a). In ΔSNOW, snow compaction is determined by the Newtonian viscosity theory; overburden due to new snow is treated as unsteady compaction; and snowmelt is distributed stepwise from top to bottom. The input of the model is snow depth measured at stations. Evaluation statistics (Fig. S3) shows that ΔSNOW simulated SWE is superior at 66 CMA and Ganjia La stations compared to SWE calculated from snow depth using fixed snow density of 0.18 g/cm^3 and SWE estimated using the logistics-5 curve developed from snow scale observations at Lindi station. It should be noted that the fixed density approach is widely used in passive microwave remote sensing to derive SWE from snow depth around the globe which obviously is one of the reasons why SWE estimation from satellite measurements has issues. The reconstructed temporally continuous daily SWE was used to evaluate the station-scale VIC simulated SWE at the 66 locations.

Macro-scale hydrological model VIC 4.2 was used to simulate snow hydrological process both at point (66 stations) and grid (0.25° ×0.25° resolution) scales over the TPP. The VIC has been widely used around the globe to study hydrological processes. In this version, the blowing snow sublimation (BSS) algorithm by Bowling et al. (2004) was activated. This algorithm accounts for the variability of wind speed, snow transport, and the sublimation related to complex terrain and land cover types in sub-grids. This algorithm requires the specification of standard deviation of terrain slope, mean wind fetch, and lag-1 autocorrelation of terrain gradients in sub-grids.

The VIC snow module includes snow interception by vegetation canopy and snow variation in sub-grid terrain through elevation-based snow bands. Here, we used a flexible number of snow bands at an elevation interval of 100 m. Depending on the terrain features in sub-grids, the number of snow bands varied from 1 to 69 in the 0.25° ×0.25° grid cells, high in the rugged periphery and low in the flat interior plains, consistent with the relief roughness (Figs. 1b, S4). Changes in temperature and precipitation with elevation for sub-grid snow bands were determined for each river basin based on

https://doi.org/10.5194/egusphere-2025-4849
Preprint. Discussion started: 8 December 2025

climate station locations and sub-grid elevation (Fig. S4). As a result, temperature lapse rate and precipitation gradient with elevation remain constants within individual snow bands of each river basin. This way, the effect of terrain variability on snow in sub-grids can be reasonably well accounted for in individual basins by the model. Snow density calculation in the VIC considers new snow compaction and overburden by aging snow. Snow albedo decays with time since the last snowfall and is represented by two sets of parameters for accumulation and melting seasons, respectively. Snowfall and rainfall are partitioned by using thresholds of daily temperature maxima and minima, respectively. Mixed snowfall and rainfall correspond to temperature falling between the two thresholds. There are 10 parameters related to snow simulation in the VIC (Table S5).

2.4 Analyses

Fig. 2 shows the modelling and analysis framework. Briefly, ΔSNOW simulated continuous SWE was evaluated using in-situ data. Sensitivity of snow parameters in the VIC was investigated using the Sobol' method at Ganjia La. The sensitive snow parameters were then calibrated automatically and validated against ΔSNOW simulated SWE at randomly selected 56 CMA stations. The calibrated and validated snow parameters at the CMA stations were subsequently extrapolated to the 0.25° ×0.25° grid cells using 1-dimension Convolutional Neural Network (1D-CNN) deep learning approach and MODIS snow cover. Using extrapolated sensitive parameter values and gridded forcings, VIC simulated SWE in 0.25° ×0.25° was further evaluated against ΔSNOW SWE at the 10 remaining CMA sites and from previous studies. Limited previous TPP snowmelt, sublimation and evaporation studies were collected and used to assess gridded VIC simulations. Statistics matrices including linear correlation coefficient (CC), root mean square error (RMSE), Nash-Sutcliffe Efficiency (NSE), relative bias in means (Pbias), and Kling-Gupta Efficiency (KGE) were used for simulation evaluation. The key steps are described in greater detail below.

Sobol' method (Sobol' 1993; Houle et al., 2017), hourly meteorological data and continuous SWE observations during May 1, 2016 – May 31, 2018 at Ganjia La station were used to identify sensitive snow parameters of the VIC. Sobol' method varies all parameters and identifies the amount that each

https://doi.org/10.5194/egusphere-2025-4849
Preprint. Discussion started: 8 December 2025

parameter contributes to the variance of the objective functions (the five statistics matrices mentioned above). In total, 576 simulations were conducted to generate the Sobol' ensemble at Ganjia La. Maximum temperature when snow falls (Tmax), minimum temperature when rain falls (Tmin), snow liquid water holding capacity (LWHC), new snow albedo (NSA), albedo decay during accumulation and melting seasons (expA1, expA2), and snow roughness length (SR) were identified to be sensitive.

Next, the Adaptive Surrogate Modeling based Optimization algorithm (ASMO, Wang et al., 2014) was used to auto-calibrate the sensitive snow parameters by comparing simulated SWE to ΔSNOW reconstructed SWE time series at randomly selected 56 stations (Fig. S5). Calibration and validation period was 1980-1994 and 1995-2009, respectively. The ASMO builds a surrogate model to represent the response of the VIC to parameter variation. It involves initial sampling, regression and adaptive sampling. The coupling of the ASMO and VIC was realized using Python. The interface of the coupled model includes the names of sensitive snow parameters, their locations in the VIC model and their value ranges, number of iteration steps, and objective functions. The optimal sets of parameter values and the corresponding objective functions were recorded for final selection.

https://doi.org/10.5194/egusphere-2025-4849
Preprint. Discussion started: 8 December 2025

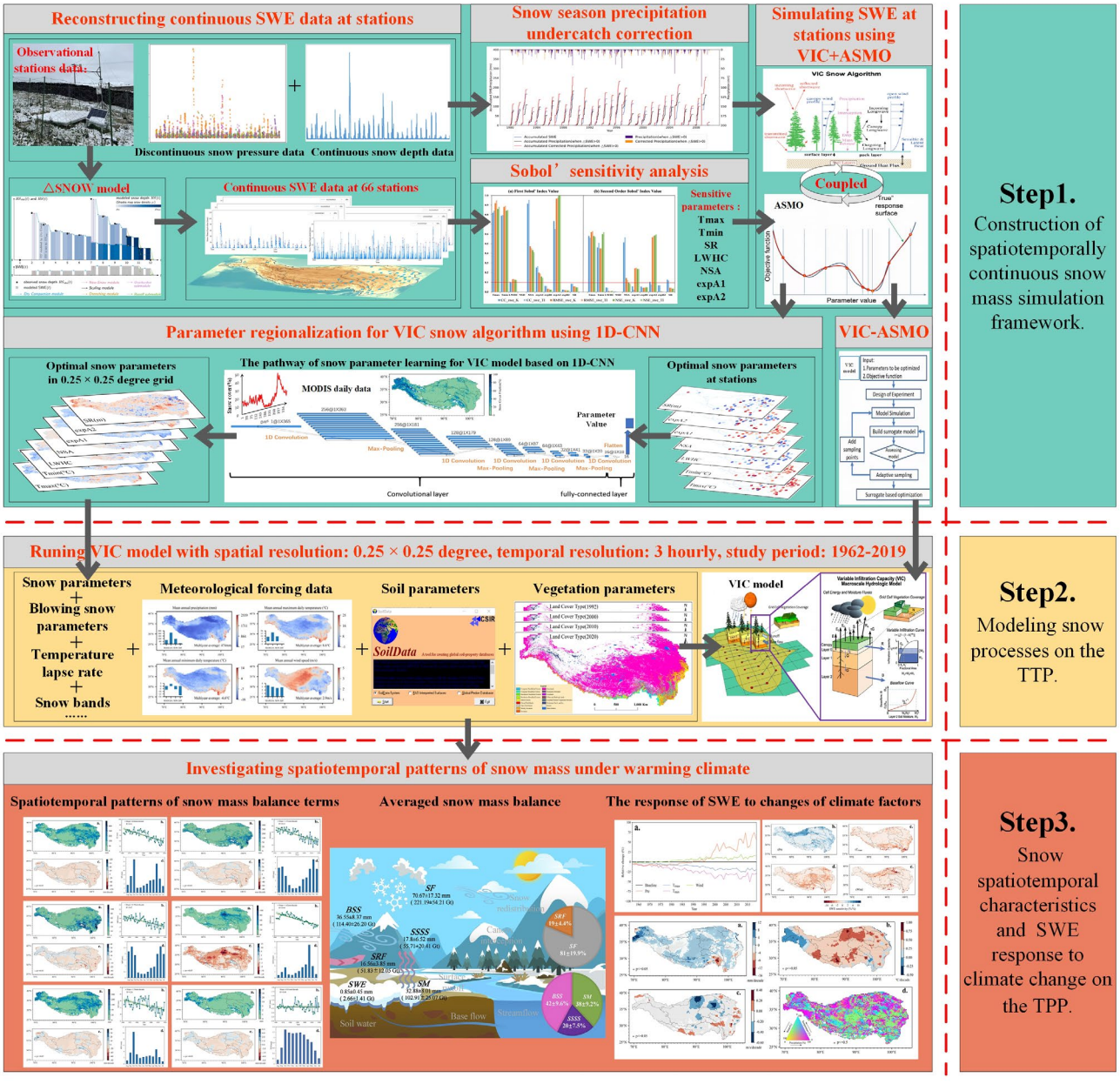

Figure 2: Schematic diagram and flowchart of the snow simulation framework developed and applied on the TPP in this study.

Using the VIC-ASMO framework, 500 runs were conducted at 56 stations to obtain the optimum parameter sets which resulted in the averaged CC of 0.8, RMSE of 1.6 mm, NSE of 0.6, Pbias of -10%, and KGE of 0.7 during the calibration period; and averaged CC, RMSE, NSE, Pbias and KGE of 0.8,

https://doi.org/10.5194/egusphere-2025-4849
Preprint. Discussion started: 8 December 2025

1.5 mm, 0.5, -6%, and 0.6, respectively, during the validation period (Fig. S6a). As an example, at Cuona station where snow amount was greater than the other stations during the calibration period, CC, RMSE, NSE, Pbias and KGE were 0.9, 5 mm, 0.8, 10%, and 0.8, respectively (Fig. S6b).

1D-CNN (Kiranyaz et al., 2021) was used to regionalize calibrated sensitive parameter values at stations to the entire TPP represented by 0.25°×0.25° grids. This is essentially a step of transferring parameter values from gauged sites to vast ungauged grid cells by using deep learning. CNN fuses the feature extraction and classification into a single learning body and optimizes the features in the training phase directly from raw data, and builds a relationship between input and output. CNN has three layers: input, hidden and output. The hidden layer consists of convolutional layer, pooling layer and fully connected layer. 1D-CNN has low computation requirement and is efficient when input data are scarce and has been applied to study outgoing longwave radiation, soil texture and drought (Zhu et al, 2022; Kiranyaz et al, 2021; Mokhtar et al, 2021).

56 stations were utilized to train 1D-CNN and the remaining 10 stations were used to test 1D-CNN (see Fig. S5 for the locations of training and test sites). Values of seven sensitive parameters were targets, and 500-m daily snow cover from MODIS at 56 stations were input for building seven 1D-CNN learning models to regionalize parameter values. In this study, the size of filter kernel was 3 and convolutional layers were 10. The number of each filter kernel was set to 256/256/128/128/64/64/32/32/16/16, respectively. 1D-CNN-based models were trained using the Adam optimization algorithm. The initial weight and learning rate were set to 0.001. The mean square error (MSE) between the learning model output and the target value served as the loss function (or cost function). In fully connected layer, ReLU and Sin activation functions were used to ensure a reasonable output range for each parameter. L1 regularization was added to the weight parameter to normalize the rationality of the model parameters and improve the efficiency of small sample learning.

To test the seven built 1D-CNN models, first snow cover time series at the remaining 10 sites were input to the seven models and then the output snow parameter values were used in the VIC to simulate SWE at the 10 test sites, which were evaluated using reconstructed SWE. Averaged CC, RMSE, NSE,

https://doi.org/10.5194/egusphere-2025-4849
Preprint. Discussion started: 8 December 2025

Pbias and KGE at the 10 sites were 0.7, 2.1 mm, 0.4, -13%, and 0.6, respectively (Fig. S6a). Although simulated SWE at the test sites were inferior to that at the training sites, the simulation was still reasonable given the relatively high CC and KGE and lower RMSE and Pbias. The spatial patterns of the values of five objective functions at the training and test stations are shown in Fig. S7. Stations in the north, west and east display better results than those in the south. Fig. S8 reveals that the values of the seven sensitive snow parameters at 66 stations are spatially heterogeneous. Tmax ranges in -5 – 5 °C, Tmin -10 – 5 °C, NSA 0.80 – 0.90, LWHC 0.02 – 0.15, and SR 0.0 – 0.03 m.

Further, using 1D-CNN learning models, sensitive snow parameter values calibrated and validated at stations were regionalized in order to simulate snow mass components for the entire TPP. At this step, because of the already large number of 0.25°×0.25° resolution grid cells (4787) covering the domain and considering the computation capability, 500-m MODIS snow cover time series was resampled to 0.25°×0.25° snow cover first and then was input to the 1D-CNN learning model to obtain VIC sensitive snow parameter values for each 0.25°×0.25° grid cell of the entire domain. It appears that the deterioration of input snow cover resolution did not affect the optimization results as parameter values at the calibrated sites are similar to those in grid cells that cover the sites (Fig.S9).

Other snow mass balance terms such as snowmelt and refrozen snow were not evaluated rigorously due to few previous studies and lack of measurements. However, given undercatch correction of snow season precipitation, adequate snow band setting, rigorous sensitive snow parameters calibration and validation, and thorough evaluation of key snow mass components in the VIC model, simulations of snowmelt and refrozen snow were considered reasonable.

Next, we analyzed the spatiotemporal patterns of VIC-simulated SWE and snow mass balance terms across the entire domain and in individual watersheds, the basic water resource management units. SWE relationships with temperature, precipitation, and wind speed were examined using multiple linear correlation. Trends were assessed with Mann-Kendall and Sen's slope, a nonparametric approach, with statistical significance level at $p<0.05$. Uncertainty in long-term mean was represented by two standard deviations of the time series. The snow year runs from August 1 in previous year to July 31 in next year,

https://doi.org/10.5194/egusphere-2025-4849
Preprint. Discussion started: 8 December 2025

aligning with annual snow phenology. Since the spatial resolution is 0.25° ×0.25°, the redistribution of snow between grids due to blowing snow is not considered in the model.

3 Results

Snow remains thin and patchy since about 70% of annual precipitation falls in the warm season (May–September) at 95% of stations in the vast Tibetan Plateau due to monsoon climate (Qin et al., 2006; Ma and Qin, 2012; Gao et al., 2023; Cuo and Zhang, 2017). Unlike North America where snow accumulates and peaks around April 1 (Hamlet et al., 2005), snowfall on the vast Tibetan Plateau is relatively limited and snow tends to melt or sublimate after each snowfall event, which hinders the buildup of maximum snowpack at the end of snow season. Hence, we use averaged SWE over snow-covered areas in snow season for monthly and annual analyses. Other snow mass components are represented by their accumulation in the entire TPP during snow season at monthly and annual steps.

3.1 SWE

Mean annual SWE is highest in the West Kunlun, Hindu Kush, Karakoram, and west Himalayas, with smaller peaks in Nyenchen Tangla, Hengduan, eastern TP, and Qilian mountains (Fig. 3a). The vast interior has little SWE, only a few millimeters at most. TPP-wide averaged annual SWE is 0.85±0.45 mm or 2.66±1.41 gigatonne equivalent of water (hereafter Gt). SWE peaks around 5000 m above sea level, with a smaller peak near 2500m above sea level, located mainly in the TPP periphery and the Pamirs (Fig. 3e). Annual SWE over the TPP shows a negligible trend of -0.01 mm/decade (1962–2019, Fig. 3c). Spatially, SWE trends range from -4.0 to 6.0 mm/decade, with 69.25% (34.09%) of the TPP showing negative (significantly negative) trends (Fig. 3b). The western and northern basins show positive trends, but only 10.77% are significant. Among the basins (Table 1), the Amu Darya (2.54 mm) and Indus (2.19 mm) in the west have the highest annual SWE, while the desert Qaidam Basin has the lowest (0.07 mm). SWE increases in the Amu Darya, Indus, and Qaidam, but significant only in the Indus. Significant declines in SWE are seen in the Ganges, Brahmaputra, Salween, Mekong, Yangtze, and Qilian Mountain basins (Table 1).

https://doi.org/10.5194/egusphere-2025-4849
Preprint. Discussion started: 8 December 2025

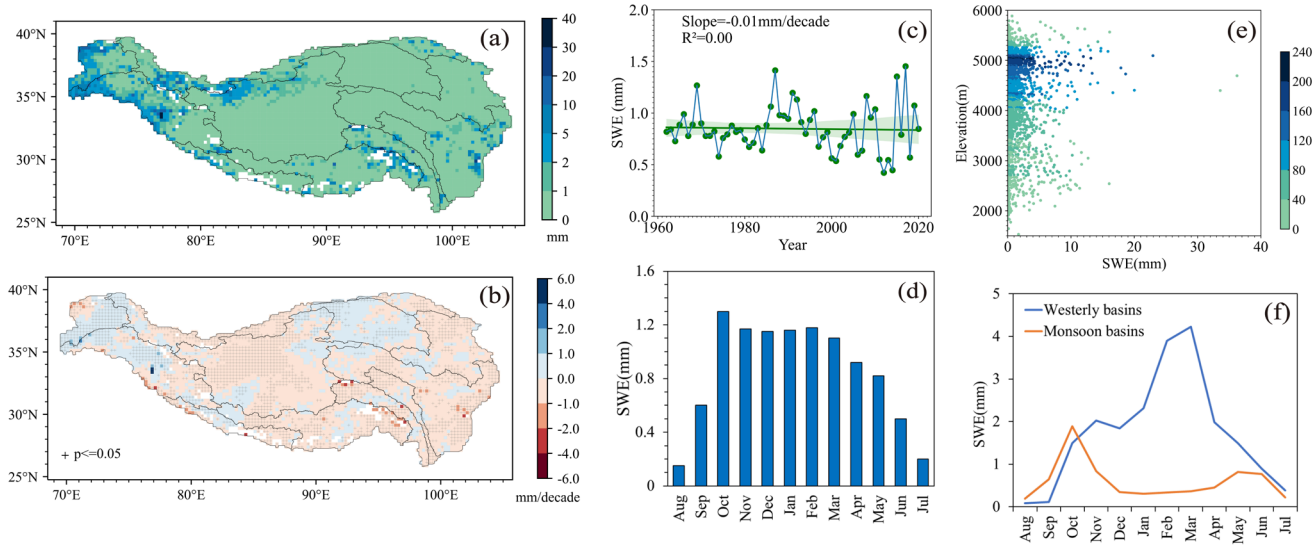

Figure 3: Spatiotemporal patterns of SWE. Mean annual SWE (a) and changes (b) during 1962-2019 over the TPP, spatially averaged annual SWE (c) and mean monthly SWE (d) during 1962-2019, density scatter plot of annual mean SWE as a function of elevation (e), and long-term mean monthly SWE for the westerly dominated and monsoon influenced climate regions (f) on the TPP. Unit is mm in (a), (c), (d), (e), (f) and mm/decade in (b). Note, blank cells in (a) and (b) represent glacial cells, + in (b) represents significance level at α=5%, and the same notations are used hereafter in spatial maps.

Using Israeli's (2007) method (see Supplementary text 1), we analyzed the impact of snowy-day precipitation, temperature, and wind speed on annual SWE via multiple linear regression. Precipitation and temperature generally increase, while wind speed decreases over the TPP in 1962-2019 (Fig. S10a–c). SWE changes are driven by precipitation in the north and west, and by temperature and wind speed in the south and center (Fig. S10d). Precipitation, temperature, and wind speed changes account for 40.9%, 33.4%, and 25.7% of SWE changes in the entire TPP, respectively, mirroring Gao et al. (2023) who conducted station analysis. Increasing SWE in the Pamirs results from increasing precipitation and decreasing temperature (Fig. S10a–b, Fig. 3b).

https://doi.org/10.5194/egusphere-2025-4849
Preprint. Discussion started: 8 December 2025

Table 1: Annual means (mm) and trends (mm/decade) of snow mass components in the 12 river basins of the TPP.

	SWE		SF		BSS		SSSS		SM		SRF	
Basins	Mean	Trend	Mean	Trend	Mean	Trend	Mean	Trend	Mean	Trend	Mean	Trend
Upper Yellow	0.26	-0.02	85.22	**-6.18**	51.99	**-3.16**	23.55	**-2.27**	23.55	**-1.39**	13.73	**-0.69**
Upper Yangtze	0.62	**-0.08**	89.93	**-5.22**	39.58	**-1.46**	21.49	**-1.23**	57.39	**-5.03**	28.32	**-2.49**
Upper Mekong	0.6	**-0.06**	78.25	**-4.11**	45.08	-1.50	15.86	**-0.91**	49.39	**-4.67**	28.48	**-3.07**
Upper Salween	1.19	**-0.23**	76.88	**+3.73**	46.22	**2.39**	14.2	0.26	51.77	**-1.88**	33.9	**-2.56**
Brahmaputra	0.87	**-0.15**	82.14	**-6.27**	33.35	**-1.88**	16.15	**-0.90**	67.67	**-5.50**	34.44	**-2.57**
Upper Ganges	0.87	**-0.12**	47.89	-1.15	19.90	0.41	17.27	**-0.82**	29.7	**-1.72**	19.43	**-1.08**
Upper Indus	2.19	**0.39**	52.45	**-2.69**	30.17	-0.34	10.11	**-1.40**	30.37	-1.48	17.2	-0.36
Upper Amu Darya	2.54	0.18	105.75	0.98	83.53	2.43	11.22	**-1.56**	25.19	**+2.29**	14.55	**+2.20**
Upper Tarim	1.49	-0.04	78.55	**-3.69**	47.53	**-1.84**	11	**-1.25**	27.86	0.31	7.32	**+0.82**
Inner TP	0.35	-0.02	52.63	**-5.16**	25.44	**-2.12**	19.8	**-2.45**	11.62	**-0.39**	3.93	**+0.20**
Qaidam	0.07	0.002	47.28	**-3.14**	22.54	**-0.65**	20.84	**-2.42**	6.55	0.08	2.59	**+0.14**
Qilian Mountain	0.72	**-0.04**	108.64	**-5.16**	64.56	**-2.27**	26.75	**-1.87**	32.65	-1.02	15.07	0.04

SWE: snow water equivalent; SF: snowfall; BSS: blowing snow sublimation; SSSS: standstill snowpack surface sublimation; SM: snowmelt; and SRF: refrozen snow. A bold number represents a statistically significant trend.

Monthly SWE averaged over the TPP peaks in October (slightly less than 1.4 mm) and then declines but remains relatively stable until March after which monthly SWE decreases rapidly and reaches a minimum in August (Fig. 3d). However, a comparison of monthly SWE between westerly circulation dominated basins (Amu Darya and Indus) and monsoon dominated basins (Yellow, Yangtze, Mekong, Salween and Brahmaputra) reveals a major peak in both regions but with different timing and magnitude (Fig. 3f). SWE peaks in October in monsoon dominated basins without much accumulation in the snow season; whereas westerly basins experience snow accumulation that peaks in March, the end of snow season. In contrast to westerly-dominated basins, snow in monsoon-dominated basins is

https://doi.org/10.5194/egusphere-2025-4849
Preprint. Discussion started: 8 December 2025

both limited in amount and short in duration, supporting the earlier statement of thin and patchy snow across the vast interior of the TPP.

3.2 Snowfall

Snowfall is a dominant input to snowpack and is calculated by partitioning precipitation using temperature thresholds of Tmax and Tmin (Fig.S8, S9). There is no measured snowfall available on the TPP, and also very few studies focus on snowfall on the TPP. One exception is Zhou et al. (2018) who used CMA observed snow pressure to retrieve snowfall and showed that in the east TPP where most stations are located snowfall ranged from 1 to 150 mm during 1961-2013, consistent with the VIC simulations during 1962-2019 (Fig. 4a).

Across the TPP, annual snowfall varies from a few millimeters in the valleys to more than 400 mm in the highlands and mountains (Fig. 4a). Mean annual snowfall is 70.67±17.32 mm when averaged over the TPP, about 221.19±54.21 Gt, which is around 12% of TPP's annual total precipitation. Annual snowfall exhibits a decrease trend during 1962-2019 and a drastic drop happened around 1997-1998 (Fig. 4b) when a major El Niño event occurred. About 87.3% (66.7%) of the TPP shows decreasing (significantly decreasing) annual snowfall (Fig. 4c). Spatially averaged snowfall peaks in May and October, but less than 16 mm in magnitude (Fig. 4d). Spatial distributions of monthly accumulated snowfall display heterogeneous patterns, and snowfall occurs primarily (little) in the periphery (vast interior) of the TPP during January-March and November-December (Fig. S11). Snowfall peaks in May and October in the majority of the interior TPP, with some areas receiving 45 mm or more in a month. In the Pamirs, snowfall starts in October and lasts till next spring. In the interior Tibetan Plateau, snowfall occurs from May through October (Fig. S11). The highest annual snowfall occurs in the Qilian Mountain, followed by the upper Indus, and the lowest happens in the Qaidam and upper Ganges (Table 1). Except for the positive trends in the upper Salween and Amu Darya, all other basins display negative trends, and most trends are statistically significant (Table 1).

https://doi.org/10.5194/egusphere-2025-4849
Preprint. Discussion started: 8 December 2025

3.3 Snow sublimation

Mean annual BSS follows snowfall patterns, high in mountains but low in the interior (Fig. 4e). Upper Yellow, Yangtze, Mekong, and Salween basins show high BSS. TPP-wide BSS peaked at 43.9 mm in 1997, then declined sharply (Fig. 4f). BSS variability mirrors that of snowfall (R^2 = 0.77, Fig. 4b). Averaged annual BSS over the TPP is 36.55±8.37 mm or 114.40±26.20 Gt. Annual BSS declines across 77.3% of the TPP, with significant trends in 47.7% of the region, mainly in the western tip, Kunlun Mountains, Qiangtang plain, and eastern TPP (Fig. 4g). The Pamirs and Nyenchen Tangla Mountains show increasing trends. BSS peaks in October (>10 mm) and is lowest in July-August (Fig. 4h).

Annually averaged SSSS is highest along the eastern Kunlun and Qilian mountains and eastern river headwaters (Fig. 4i), and is generally lower than BSS on the TPP. Spatially averaged annual SSSS is 17.8±6.52 mm or 55.71±20.41 Gt, about half of BSS. SSSS declined after the late 1970s, with a sharp drop around 1997 due to reduced snowfall (Fig. 4j, 4b; R^2 of 0.81). About 92.0% (76.5%) of the TPP exhibits decreasing (significantly decreasing) SSSS trends, with the steepest decline found in the eastern Kunlun (Fig. 4k). SSSS peaks in May (>5 mm) and remains lower than BSS year-round (Figs.4l, 4h).

On an annual average, BSS is greater than SSSS in all basins (Table 1). The highest BSS is in the upper Amu Darya and the lowest in the upper Ganges (Table 1). All basins see decreased BSS and SSSS except for the upper Salween, Ganges and Amu Darya (Table 1).

https://doi.org/10.5194/egusphere-2025-4849
Preprint. Discussion started: 8 December 2025

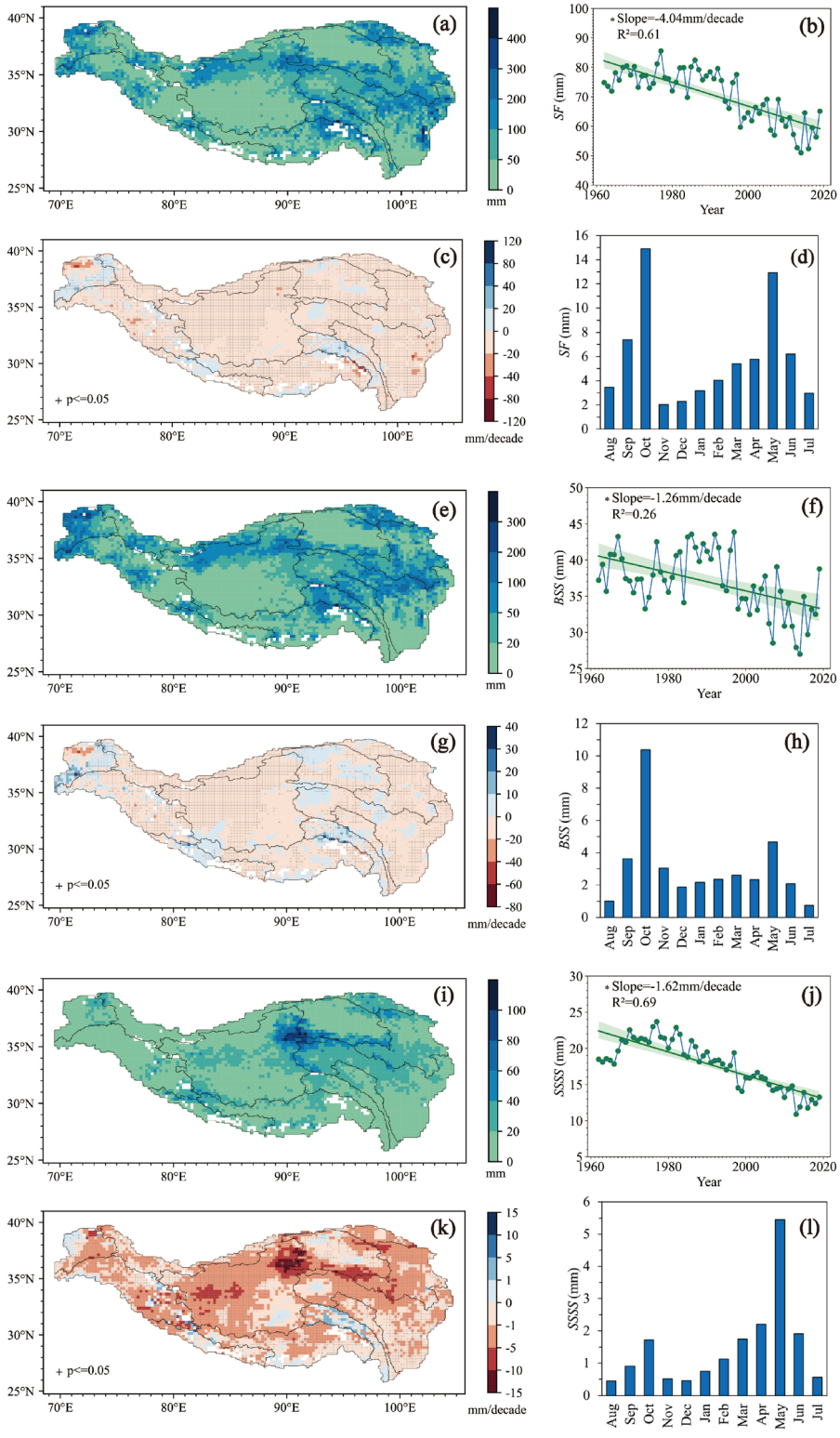

https://doi.org/10.5194/egusphere-2025-4849
Preprint. Discussion started: 8 December 2025

Figure 4: Spatiotemporal patterns of snowfall, sublimation and evaporation during 1962-2019 over the TPP. Annual snowfall (SF) (a) and changes (c), spatially averaged annual SF (b) and mean monthly SF (d); annual blowing snow sublimation (BSS) (e) and changes (g), spatially averaged annual BSS (f) and mean monthly BSS (h); annual standstill snowpack surface sublimation (SSSS) (i) and changes (k), spatially averaged annual SSSS (j) and mean monthly SSSS (l). Units are mm in (a), (b), (d), (e), (f), (h), (i), (j), (l) and mm/decade in (c), (g), (k).

3.4 Snowmelt and refrozen snow

Refrozen snow (SRF) includes snow deposition and refrozen snowmelt. Annual snowmelt (SM) and SRF display similar spatial patterns, high in the southeast while low in the interior, and SM is generally larger than SRF, with SM approximately being double of SRF in magnitude (Fig. 5a, e). Regionally averaged annual SM and SRF decrease significantly at 1.91 and 0.79 mm/decade, respectively (Fig. 5b, f). Spatially, about 74.6% (46.8%) and 66.8% (40.9%) sees decreasing (significantly decreasing) SM and SRF, respectively (Fig. 5c, g). The western TPP, however, experiences significant increase trends in SM and SRF. SM and SRF monthly patterns are also very similar, showing low values in snow season and high values in melting season especially in June to September (Fig. 5d, h). Annual mean SM and SRF are the highest in Brahmaputra and lowest in Qaidam (Table 1). Most basins except for upper Amu Darya exhibit significant decreasing trends of SM; whereas upper Amu Darya, upper Tarim, Inner basins and Qaidam all experience significantly increasing SRF (Table 1).

https://doi.org/10.5194/egusphere-2025-4849
Preprint. Discussion started: 8 December 2025

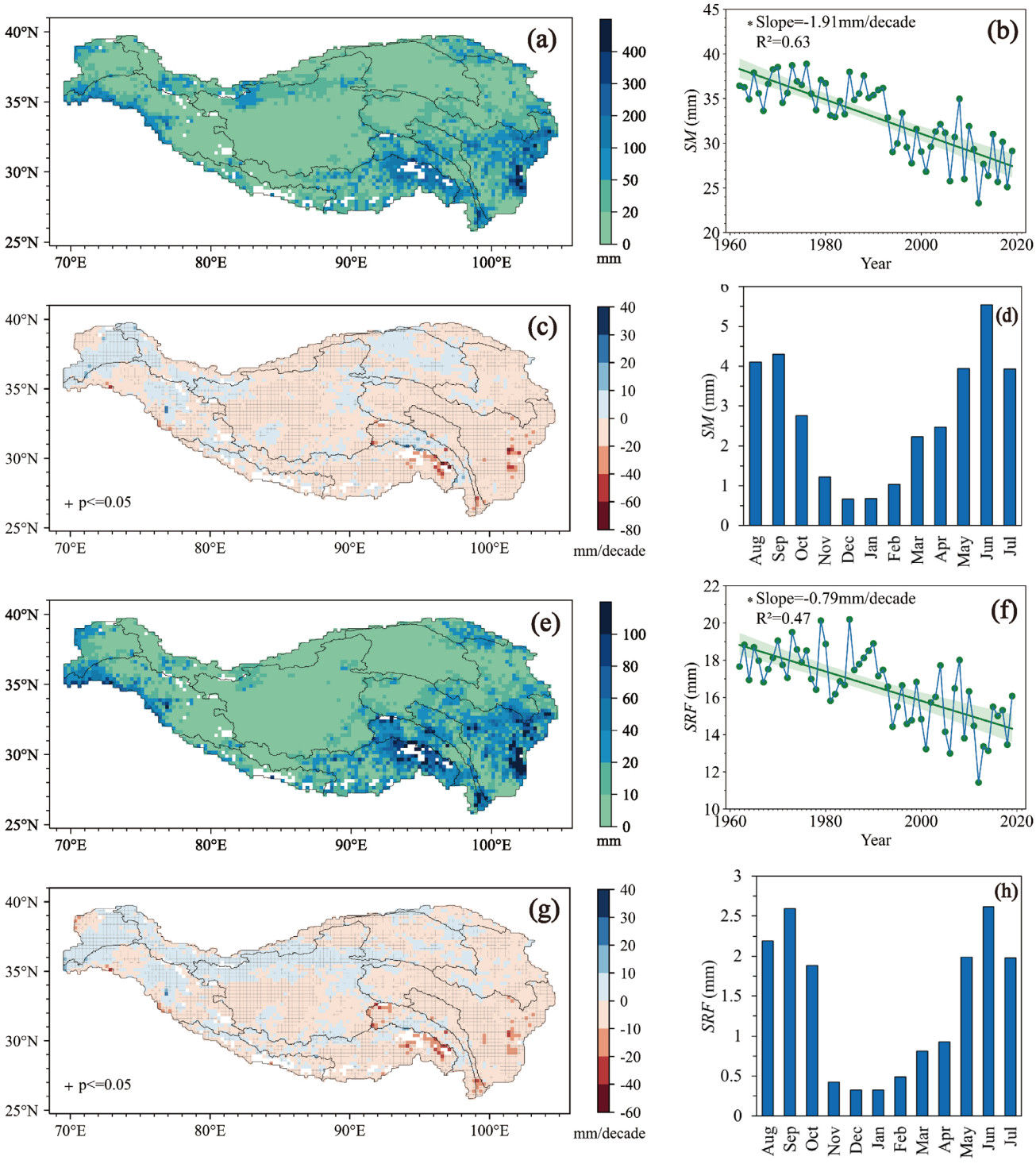

https://doi.org/10.5194/egusphere-2025-4849
Preprint. Discussion started: 8 December 2025

Figure 5: Spatiotemporal patterns of snowmelt and refrozen snow. Mean annual snowmelt (a) and changes (c) during 1962-2019 over the TPP, spatially averaged annual snowmelt (b) and monthly snowmelt (d); mean annual refrozen snow (e) and changes (f) during 1962-2019 over the TPP, spatially averaged annual refrozen snow (g) and monthly refrozen snow (h). Units are mm in (a), (b), (d), (e), (f) and (h) and mm/decade in (c) and (g).

3.5 Snow mass balance

The above variables constitute the main components of the snow mass balance given as Eq. (3):

$$SF + SRF = SM + BSS + SSSS + \frac{\delta SWE}{\delta t} \quad (3)$$

where $\delta SWE / \delta t$ is the change of SWE in one snow year, which is generally very small and can be ignored on the TPP.

As shown above, averaged over the TPP, VIC simulated annual snowfall is 70.67±17.32 mm or 221.19±54.21 Gt, and annual refrozen snow is 16.56±3.85 mm or 51.83±12.05 Gt. Total snow water resource or input of the snow pack (left terms in Eq. (3)) on the TPP is the sum of refrozen snow and snowfall, which is 273.02±66.26 Gt. Annual snowmelt on the TPP is 32.88±8.01mm or 102.91±25.07 Gt. The available annual snow water resource is the sum of snowmelt and SWE, which is 105.57±26.48 Gt or 105.57±26.48 billion m^3, about 38.7±0.2% of snow input (Fig. 6).

https://doi.org/10.5194/egusphere-2025-4849
Preprint. Discussion started: 8 December 2025

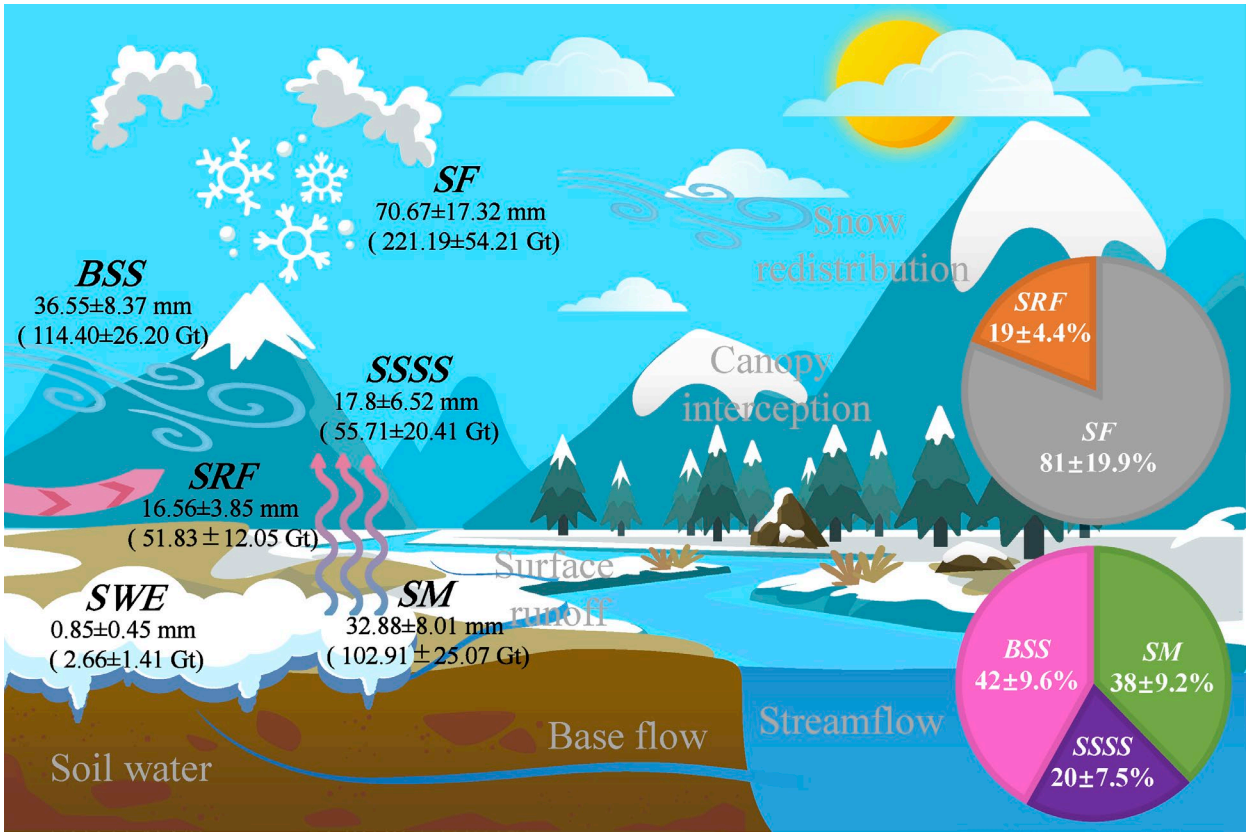

Figure 6: The amount and proportions of snow mass balance terms on the TPP. SF: snowfall; BSS: blowing snow sublimation; SSSS: standstill snowpack surface sublimation; SRF: refrozen snow; SM: snowmelt; and SWE: snow water equivalent.

Assuming that all available annual snow water resources contribute to annual discharge of all river basins on the TPP as a potential, and using the total river discharge of 656±23 billion m^3 in 2018 from Wang et al. (2021) and long-term average annual total discharge of ~550 billion m^3 at the outlets in the periphery of the TPP over the past decades from Zhang et al. (2013), Poudel et al. (2022), Cuo et al. (2014), and Hou et al. (2023) as approximations, the potential snow contribution to the total stream discharge of all rivers is estimated to be around 12-19% annually, on average. However, the contribution can be high in specific locations and months. For example, more than 45% of annual discharge in sub-basins of Brahmaputra and Tarim is from snow (Cuo et al., 2014). Snow water contribution to annual streamflow in Amu Darya sub-basins in the west TPP varies in 15-50% (Hou et

https://doi.org/10.5194/egusphere-2025-4849
Preprint. Discussion started: 8 December 2025

al., 2023). Streamflow in April and May is also significantly and positively correlated with early winter and spring snow depth in sub-basins of upper Brahmaputra (Cuo et al., 2019).

Annual snow sublimation and evaporation, a loss from the perspective of water resource, is the sum of BSS (114.40±26.20 Gt) and SSSS (55.71±20.41 Gt), which is 170.01±46.61 Gt. This is greater than available water resource of 105.57±26.48 Gt and equals to 62.3±1.6% of annual snow input (Fig. 6), even higher than the reported percentage of 15-41% in the Canadian prairies (Pomeroy and Gray, 1995). Hence, annually averaged over the TPP, snow contribution to atmospheric water vapor is much higher than that to available water resources over the TPP. Therefore, snow sublimation and evaporation must be considered in snow water resource estimation to avoid overestimation of snow contribution to stream discharge on the TPP. Further questions to ask include how snow's contribution to atmospheric water vapor compares with that from other local land cover types, such as vegetation and bare land, as well as moisture transported from outside the TPP—an issue that deserves future research.

4 Discussion

4.1 Climate effects of snow change

On the TPP, snow not only contributes more to atmospheric water vapor than to available water resource but also acts as an important modulator of climate system and weather. Pu and Xu (2009) reported that during 1979-2014 snow cover on the TPP is highly heterogenous spatially and snow cover occurs year-round in about 10% of the TPP. Li et al. (2018) reported that high snow cover variability in snow season on the TPP is related to East Asian upper-level westerly jet variability at 3-8 days later which subsequently affects weather on the TPP and its surroundings. Moreover, snow cover reduces diurnal fluctuations of soil temperature, hence diurnal soil freeze-thaw cycles, due to albedo effect and low thermal conductivity of snow (Li et al., 2024). Li et al. (2018), Chen et al. (2021), and Ma et al. (2023) found that the TPP in general experiences decreasing snow cover. Li et al. (2018) reported that snow cover decreasing rates (-0.33– -0.13 %/year) in January-May are greater than those in the other months. Given positive albedo feedback effect, reduced snow cover in cold season could enhance warming in winter which is already happening on the TPP (Yang et al., 2010). Cuo et al. (2021) found

https://doi.org/10.5194/egusphere-2025-4849
Preprint. Discussion started: 8 December 2025

that maximum and minimum air temperature in December-January-February warmed at 0.04 and 0.06 ℃/year during 1957-2019, respectively, the greatest among the four seasons. As there is essentially no vegetation canopy on the vast TPP in winter, snow cover reduction is the dominant factor for the winter warming amplification on the TPP, similar to the Arctic Amplification (Screen and Simmonds, 2010; Cohen et al., 2020). Snow cover reduction will not only affect local climate conditions but also have far-reaching effects on the Indian, eastern and southern China monsoon rainfall. Widespread thin snow cover impacts weather and climate locally and remotely through the Blanford's mechanism whereby the combined snow albedo effect, reduced sensible heat flux and longwave flux cool the troposphere and modulate the atmospheric circulations. Wu and Kirtman (2007) found that spring snow cover on the TPP displays moderate positive correlation with spring rainfall in south China during the ENSO (El Niño – Southern Oscillation) events. Observations and simulations all show that snow cover anomaly in fall-winter-spring on the TPP leads to rainfall anomaly in east China (Wang et al., 2018). Also, winter snow cover on the TPP exhibits a strong negative relationship with Indian summer monsoon rainfall in the absence of ENSO because of the Blanford's mechanism (Turner and Slingo, 2011).

4.2 Quality of the snow simulation

The complex terrain in the sub-grid of the 0.25° ×0.25° grid cells on the TPP was represented by 100-m-interval snow bands. This treatment improved not only snow simulation in the complex terrain of the TPP with high relief roughness (Fig. 1b) by using a relatively large number of snow bands, but also the computational efficiency in the inner TPP with low relief roughness by using fewer snow bands (Fig. S4). The quality of VIC simulated SWE was carefully ensured using observation data and advanced techniques through a series of steps detailed in Analysis: 1) correcting precipitation undercatch in snow season, 2) using temporally continuous SWE simulated by ΔSNOW forced by observed snow depth and evaluated by observed SWE, 3) automatic calibration of VIC sensitive snow parameters using ASMO, and 4) regionalization of calibrated sensitive VIC snow parameter values from stations to grid cells using 1D-CNN and MODIS snow cover. The five statistic matrices related to SWE evaluation are satisfactory according to the criterion set by Moriasi et al. (2007).

https://doi.org/10.5194/egusphere-2025-4849
Preprint. Discussion started: 8 December 2025

Our study shows that snow mass is limited in the vast interior TPP which is also confirmed by previous studies. Zhang et al. (2015) showed that accumulated SWE in December-January-February was less than 3 mm for most years during 1979-2010 on the TPP and SWE dropped drastically around 1987/1988, similar to VIC simulations (Fig. 3c). Li et al. (2021) also showed an annual mean snow depth of only 2-3 cm during 1982-2017 at 88 CMA stations on the TPP. Ma and Qin (2012) used observed snow depth (cm) and snow pressure (g/cm^2) from the CMA to calculate snow density (g/cm^3) and then estimated SWE for the entire China during 1957-2009. They noted mean annual SWE of 0.4 mm over the Tibetan Plateau, which is in the same order of magnitude as VIC simulated mean annual SWE and falls within VIC simulated uncertainty range (0.85±0.45 mm). Slightly higher mean SWE simulated by VIC stems from the differences in study area and period. The Pamirs and the Tibetan Plateau have different climates. Under year-round westerly control, the majority of annual precipitation falls in winter and spring in the Pamirs when snow can accumulate and melt during late spring and summer (Figs.S11, 3f). Precipitation in the Tibetan Plateau is dominated by monsoons; while May–June and September–October are snow seasons, snowfall is limited and tends to sublimate, evaporate or melt after each snowfall event, preventing snow accumulation during snow season (Figs.S11, 4d, 4h, 4i, 5d). This is the reason why March or April SWE cannot represent annual snow water resource and SWE is very low in the Tibetan Plateau.

Gao et al. (2023) estimated the annual snow water resource by using the accumulated maximum SWE from each snow event, based on SWE derived from snow depth observations. For comparison, we used their approach and obtained VIC simulated annual accumulated maximum SWE. As shown in Fig. S12, high accumulated SWE maximum is located in the west, headwaters of the Salween and Mekong, portions of the Yangtze and Yellow rivers, and the west Kunlun and Qilian. Since Gao et al. (2023) used station data inside China, their spatial coverage is limited. But the spatial distributions of accumulated SWE maximum in the eastern TPP is similar in both studies, with magnitude ranging in 20-100 mm (see their Fig. 5).

A few studies used energy balance, bulk aerodynamic theory and sophisticated snow models to calculate snow sublimation on the TPP (Table 2). We compared the ratios of total snow sublimation

https://doi.org/10.5194/egusphere-2025-4849
Preprint. Discussion started: 8 December 2025

(BSS+SSSS) to snowfall (SF) and BSS to total snow sublimation between current study and previous studies at eleven sites located on the TPP (Table 2, Fig. S13). In general, VIC simulated (BSS+SSSS)/SF ratios are close to previous studies at the co-located sites. VIC simulated BSS/(BSS+SSSS) also matches the values from previous studies at the co-located sites except for sites 4 and 11. VIC simulated December-January-February snow sublimation and evaporation on the TPP is within 10 mm (Figs.4d, 4h, 4l) which is also similar to what Zhang et al. (2015) reported for 1979-2010.

Table 2: Snow sublimation simulated by VIC in this study compared with previous studies on the TPP.

	This study		Previous study			
	F1(%)	F2(%)	F1(%)	F2(%)	Methods	Reference
1	55.3	66.3	50.0	-	ARIMA and D-IUH model	Paix et al., 2012
2	83.0	63.0	high	-	Energy balance method	Zhang et al., 2013
3	56.7	52.7	47.4	50.7	CRHM model	Zhou et al., 2014
4	72.8	82.2	68.8	41.5	Energy balance method	Li et al., 2009; 2012
5	46.2	34.6	38.9	-	GBEHM model	Li et al., 2019
6	28.2	13.9	21.0	-	Bulk-aerodynamic method	Stigter et al., 2018
7	97.2	77.6	42.5-100.0	-	Heat budget method	Ueno et al., 2007
8	96.8	22.1	100.0	20.3	VIC model	Sahadeep, 2019
9	91.9	37.6	84.5	36.42		
10	32.2	16.8	31.25	15.94		
11	89.6	80.6	62.92	1.52		

F1=(BSS+SSSS)/SF; F2=BSS/(BSS+SSSS); "high" is used when no exact value is available; "-" means no reported values from the other studies.

VIC-simulated and station-based snowfall (Zhou et al., 2018, their Fig. 2a) in the eastern TPP show similar annual amount, ranging from 1 to 200 mm (Fig. 4a). Yang et al. (2022) reported annual snowmelt of 115 Gt on the TPP, together with Ma and Qin (2012) who obtained 0.4 mm annual mean SWE, the available water resource from previous studies falls within the range reported here. These comparisons and analyses demonstrate that VIC simulated snow is credible in general.

https://doi.org/10.5194/egusphere-2025-4849
Preprint. Discussion started: 8 December 2025

4.3 Uncertainty

All land surface modeling results contain uncertainties related to model physical processes, model parameter values and meteorological forcing data. The uncertainty in model physical processes is usually examined by using multiple schemes or models. For example, snow accumulation is sensitive to processes like surface heat exchange, rain and snow partition, low boundary conditions of soil temperature, and the first layer of snow or soil temperature scheme in the Noah-MP model (You et al, 2019). Marked differences in snow albedo parameterization schemes in the Noah, VIC, snow-atmosphere-soil transfer model, Land Ecosystem-Atmosphere Feedback models, Noah-MP, and Community Land Model (CLM) result in different SWE peak, timing, and duration in forest covered complex terrain in Colorado headwaters of the USA (Chen et al, 2014). Since this study used only one model, uncertainty in a single model simulation would be expected. However, in this study, snow season precipitation, model parameters, and snow processes are rigorously evaluated which results in credible model simulations. What is further reassuring is that the VIC has already been successfully applied on the TPP and other cold regions with good performance (e.g., Zhang et al, 2015; Cuo et al, 2013b).

Brun et al. (2013) used the Crocus snowpack model to evaluate two meteorological forcing datasets: the European Centre for Medium-Range Weather Forecasts (ECMWF) Interim reanalysis (ERA-Interim) and the Princeton University Global Forcing dataset (PGF) in northern Eurasia. They found that there were significant differences in snow depth, snow water equivalent, snow season onset and end time, and snow density between the two sets of simulations driven by two different forcings. Liu et al. (2023a) found that meteorological forcing had the greatest impact on snow depth simulations in the CLM, followed by the snow parameterization scheme. Below we focus on forcing related uncertainty in VIC's SWE simulations.

In this study, the averaged coefficient of determination (R^2) of the multiple linear regression between all meteorological forcings and annual SWE over the TPP is 0.64 ($p<0.05$), indicating that VIC simulated SWE is highly correlated with model forcings. Further, the response of SWE to changes in each forcing variable is investigated through the design of detrended scenarios over 1962-2019 (see Supplementary

https://doi.org/10.5194/egusphere-2025-4849
Preprint. Discussion started: 8 December 2025

Material for the details; Schaake, 1990). Fig. 7a shows that, on average, SWE on the TPP increased due to rising precipitation and declining wind speed during 1962-2019 (Fig. S15a, d), while increasing maximum (T_{max}) and minimum (T_{min}) temperature (Fig. S15b, c) reduced SWE on the TPP. SWE responses to changes in precipitation (εPre), temperature maxima (εT_{max}), temperature minima (εT_{min}) and wind speed (εWind) are 6.21, -1.17, -1.38 and -0.76, respectively. This means that 10% increase (decrease) in precipitation (wind speed) would increase SWE by 62.1% (7.6%) while 10% increase in maximum (minimum) air temperature would reduce SWE by 11.7% (13.8%). In other words, 1℃ increase in T_{max} and T_{min} would decrease SWE by 14.84% and 17.49%, respectively. Therefore, over 1962-2019 precipitation changes have exerted the greatest impact on annual SWE, followed by changes in minimum and maximum air temperature over the TPP on average. Wind speed changes show the least impact on SWE.

https://doi.org/10.5194/egusphere-2025-4849
Preprint. Discussion started: 8 December 2025

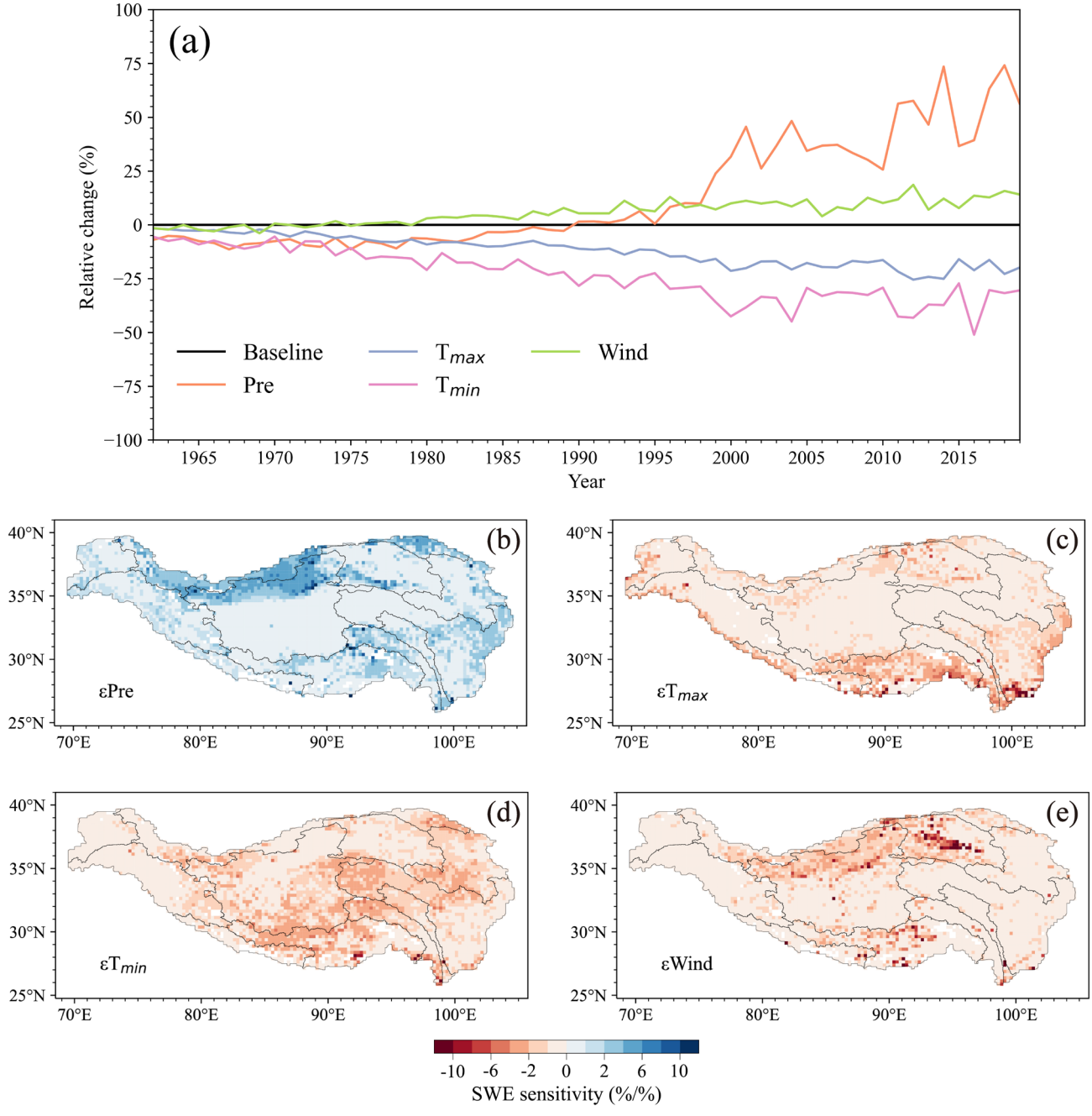

Figure 7: The response of SWE to changes of climate factors. Time series of TPP averaged SWE changes in response to changes in forcing (a), spatial distributions of SWE sensitivity to changes in precipitation (b), temperature maxima (c) and temperature minima (d), and wind speed (e) during 1962-2019

https://doi.org/10.5194/egusphere-2025-4849
Preprint. Discussion started: 8 December 2025

The responses of SWE to changes in forcings are found to be spatially diverse. Fig. 7b, c, d, e and Table 3 show that the upper Tarim and west Kunlun display the highest εPre, followed by the upper Salween, Nyenchen Tangla, Qilian and east Kunlun Mountains and the eastern TPP. The Brahmaputra, Ganges and lower Yangtze rivers show large εT_{max}. Except for the Brahmaputra, upper Ganges, lower Yangtze and Amu Darya basins, SWE in most basins is more responsive to T_{min} than to T_{max}. εWind is particularly high in the Qaidam Basin, northern inner TPP and southern TPP. Hence, uncertainties in precipitation, T_{min}, T_{max} and wind speed will propagate to SWE simulations in these sensitive locations on the TPP. Nonetheless, the quality of the forcings was evaluated at independent stations widely spread on the TPP and proved to be reliable (Table S1, S2).

Table 3. SWE sensitivity to changes in forcings in the 12 basins during 1962-2019.

Basins	SWE sensitivity			
	εPre	εT_{max}	εT_{min}	εWind
Upper Yellow	1.46	-0.62	-1.48	-0.35
Upper Yangtze	1.66	-1.27	-1.31	-0.36
Upper Mekong	1.49	-1.15	-1.38	-0.42
Upper Salween	2.42	-1.07	-2.03	-0.47
Brahmaputra	1.64	-2.28	-1.77	-1.07
Upper Ganges	1.28	-2.09	-1.15	-0.71
Upper Indus	1.15	-0.74	-0.85	-0.33
Upper Amu Darya	1.15	-1.12	-0.32	-0.18
Upper Tarim	3.77	-0.89	-0.90	-1.07
Inner Tibetan Plateaus	2.97	-0.64	-1.37	-1.08
Qaidam	1.89	-0.99	-0.86	-2.08
Qilian Mountain	3.29	-0.94	-1.56	-0.83

4.4 Evaluation of remote sensing SWE using VIC simulated SWE

As an example of the application of VIC simulated SWE, we evaluated the SWE products from FY3 and NASA-HMA, which were not evaluated by Bian et al. (2019). FY3 mean annual SWE is high in the eastern TPP and the Pamirs (Fig. S14a), while NASA-HMA shows high values in the Nyenchen Tangla,

https://doi.org/10.5194/egusphere-2025-4849
Preprint. Discussion started: 8 December 2025

Karakoram, western Himalayas and western Kunlun (Fig. S14b), indicating that FY3 and NASA-HMA exhibit different mean annual SWE spatial patterns. Consistent with Bian et al. (2019), our results show that the FY3 and NASA-HMA products significantly overestimate SWE across most of the TPP compared to VIC simulations, with mean annual SWE values of 2.90 mm for FY3 and 6.95 mm for NASA-HMA—one order of magnitude higher than VIC simulations (Fig. S14c, d). Such comparisons illustrate that passive microwave remote sensing SWE products do need improvement for the TPP. The overestimation may stem from several factors: (1) weak microwave emission signals and coarse spatial resolution that mask sub-grid variability; (2) brightness temperature retrieval algorithms designed for flat, homogeneous surfaces, which are not suitable for complex terrain; (3) omission of terrain-related effects such as shadow, slope, and aspect that influence microwave emission over the TPP; and (4) pixel saturation when snow depth exceeds 150–200 mm (Dozier et al., 2016). Additionally, a key limitation not addressed by Dozier et al. (2016) is that many remote sensing products (e.g., GlobSnow) estimate SWE using a fixed snow density.

5 Conclusions

In summary, a novel, effective and reliable snow simulation framework that incorporates in-situ and satellite observations, point-based ΔSNOW, point- and grid-based VIC models, Sobol' sensitivity analysis, ASMO automatic calibration, and 1D-CNN deep learning methods has been developed to investigate snow mass components on the TPP. The unique features of the framework include regionalization of sensitive snow parameter values calibrated from point locations to grid cells using 1D-CNN deep learning approach (see Supplementary Material), implementation of flexible 100-m elevation interval snow bands in sub-grid cells, and incorporation of blowing snow and standstill snowpack surface sublimation and evaporation schemes. This study produced two sets of good quality daily snow data at two spatial scales. The first is ΔSNOW model simulated temporally continuous SWE at 66 stations for 1980-2009. The second is VIC simulated spatiotemporally continuous snow mass balance terms at 0.25° ×0.25° resolution during 1962-2019 for the entire TPP. These datasets can be used to study snow spatiotemporal characteristics and evaluate satellite, reanalysis and other model-based datasets on the TPP.

https://doi.org/10.5194/egusphere-2025-4849
Preprint. Discussion started: 8 December 2025

Over 1962-2019, mean annual snowfall is 70.67±17.32 mm, refrozen snow is 16.56±3.85 mm, snowmelt is 32.88±8.01 mm, blowing snow sublimation is 36.55±8.37 mm, standstill snowpack surface sublimation and evaporation is 17.8±6.52 mm, and SWE is only 0.85±0.45 mm. Snow sublimation and evaporation account for about 62% of snow pack input. Annual snow water resources (snowmelt + SWE) represent ~38% of annual snow input, potentially contributing 12–19% to annual discharge at basin outlets along the TPP edge. On an annual scale, snow plays a modest role in supplying water resources across the TPP, but it contributes substantially more to atmospheric water vapor through sublimation and evaporation.

From 1962 to 2019, the TPP experienced an overall decline in snow mass components, marked by spatial variability, which will influence weather and climate patterns locally as well as remotely in southern and eastern China and India. Regionally averaged monthly SWE shows a single peak in both westerly and monsoon-dominated basins, though the timing and magnitude differ notably between the two climatic zones. In the westerly-influenced Pamirs, snow accumulates throughout winter and spring, with SWE peaking in March, making SWE a key indicator of snow water resources in this region. In contrast, in the monsoon-dominated areas of the Tibetan Plateau, snow usually melts, sublimates, or evaporates after each snowfall event, thus preventing sustained accumulation; as a result, snowmelt rather than SWE serves as the primary form of snow water resource in these areas. SWE variations are mainly driven by precipitation in the northern and western TPP, while temperature and wind speed are the dominant factors in the central and southern areas. Overall, annual SWE is most sensitive to precipitation changes and less responsive to variations in minimum and maximum temperatures.

***Data availability**:* All raw data can be provided by the corresponding authors upon request.

***Author contributions**:* CL conducted analyses, data collection, visualization and wrote manuscript; LC designed study, acquired funding, wrote and edited manuscript; YZ revised manuscript; XZ analyzed data; XL analyzed data; MH analyzed data; AW provided data. LL provided data. The authors declare that they have no competing interests. All authors read and approved the final manuscript.

https://doi.org/10.5194/egusphere-2025-4849
Preprint. Discussion started: 8 December 2025

***Competing interests**:* The authors declare that they have no conflict of interest.

***Financial support**:* This work was supported by Qinghai Key Research and Development Program (Grant No. 2024-SF-142), Key Research and Development Program of Tibetan Autonomous Region (Grant No. XZ202401ZY0050), and National Natural Science Foundation of China (Grant No. 42371130).

References

Barnett, T. P., Adam, J. C. and Lettenmaier, D. P.: Potential impacts of a warming climate on water availability in snow dominated regions, Nature., 438, 303-309, https://doi.org/10.1038/nature04141, 2005.

Bian, Q., Xu, Z., Zhao, L., Zhang, Y., Zheng, H., Shi, C., Zhang, S., Xie, C., Yang, Z.: Evaluation and intercomparison of multiple snow water equivalent products over the Tibetan Plateau, J. Hydrometeorol., 20, 2043–2055, https://doi.org/10.1175/JHM-D-19-0011.1, 2019.

Bormann, K. J., Brown, R. D., Derksen, C. and Painter, T.: Estimating snow-cover trends from space, Nat. Clim. Change., 8, 924–928, https://doi.org/10.1038/s41558-018-0318-3, 2018.

Bowling, L., Pomeroy, J. W., Lettenmaier, D. P.: Parameterization of blowing-snow sublimation in a macroscale hydrology model, J. Hydrometeorol., 5, 745–762, https://doi.org/10.1175/1525-7541(2004)005<0745:POBSIA>2.0.CO;2, 2004.

Brun, E., Voinnet, V., Boone, A., Decharme, B., Peings, Y., Valette, R., Karbou, F., Morin, S.: Simulation of Northern Eurasian local snow depth, mass, and density using a detailed snowpack model and meteorological reanalyses, J. Hydrometeorol., 14, 203–219, https://doi.org/10.1175/JHM-D-12-012.1, 2013.

Chai, Y., Miao, C. Y., Gentine, P., Mudryk, L., Thackeray, C. W., Berghuijs, W. R., Wu, Y., Fan, X., Slater, L., Sun, Q., Zwiers, F.: Constrained Earth system models show a stronger reduction in future Northern Hemisphere snowmelt water, Nat. Clim. Change., 15, 514–520, https://doi.org/10.1038/s41558-025-02308-y, 2025.

https://doi.org/10.5194/egusphere-2025-4849
Preprint. Discussion started: 8 December 2025

Chen, F., Barlage, M., Tewari, M., Rasmussen, R., Jin, J., Lettenmaier, D. P., Livneh, B., Lin, C., Miguez-Macho, G., Niu, G. Y., Wen, L., Yang, Z. L.: Modeling seasonal snowpack evolution in the complex terrain and forested Colorado headwaters region: A model intercomparison study, J. Geophys. Res. Atmos., 119, 13795–13819, https://doi.org/10.1002/2014JD02216, 2014.

Chen, X.; Yang, Y.; Ma, Y.; Li, H.: Distribution and Attribution of Terrestrial Snow Cover Phenology Changes over the Northern Hemisphere during 2001–2020, Remote Sens., 13, 1843, https://doi.org/10.3390/rs13091843, 2021.

Cohen, J., Zhang, X., Francis, J., Jung, T., Kwok, R., Overland, J., Ballinger, T. J., Bhatt, U. S., Chen, H. W., Coumou, D., Feldstein, S., Gu, H., Handorf, D., Henderson, G., Ionita, M., Kretschmer, M., Laliberte, F., Lee, S., Linderholm, H. W., Maslowski, W., Peings, Y., Pfeiffer, K., Rigor, I., Semmler, T., Stroeve, J., Taylor, P. C., Vavrus, S., Vihma, T., Wang, S., Wendisch, M., Wu, Y., Yoon J.: Divergent consensuses on Arctic amplification influence on midlatitude severe winter weather, Nat. Clim. Change., 10, 20–29, https://doi.org/10.1038/s41558-019-0662-y, 2020.

Cuo, L., Zhang, Y., Wang, Q., Zhang, L., Zhou, B., Hao, Z., Su F.: Climate change on the Northern Tibetan Plateau during 1957–2009: Spatial patterns and possible mechanisms, J. Clim., 26, 85–109, https://doi.org/10.1175/JCLI-D-11-00738.1, 2013a.

Cuo, L., Zhang, Y., Gao, Y., Hao, Z. and Cairang, L.: The impacts of climate change and land cover/use transition on the hydrology in the upper Yellow River Basin, China, J. Hydrol., 502, 37–52, https://doi.org/10.1016/j.jhydrol.2013.08.003, 2013b.

Cuo, L., Zhang, Y., Zhu, F. and Liang, L.: Characteristics and changes of streamflow on the Tibetan Plateau: A review, J. Hydrol. Reg. Stud., 2, 49–68, https://doi.org/10.1016/j.ejrh.2014.08.004, 2014.

Cuo, L. and Zhang, Y.: Spatial patterns of wet season precipitation vertical gradients on the Tibetan Plateau and the surroundings, Sci. Rep., 7, 5057, https://doi.org/10.1038/s41598-017-05345-6, 2017.

Cuo, L. Li, N., Liu, Z., Ding, J., Liang, L., Zhang Y.: Warming and human activities induced changes in the Yarlung Tsangpo basin of the Tibetan plateau and their influences on streamflow, J. Hydrol. Reg. Stud., 25, 100625, https://doi.org/10.1016/j.ejrh.2019.100625, 2019.

https://doi.org/10.5194/egusphere-2025-4849
Preprint. Discussion started: 8 December 2025

Cuo, L., Liu, Z. and Hou, M.: Climate change over the Tibetan Plateau and its effects on environmental and society, Ecosystems of Three River Source Regions., 27, 26–37, 2021.

Dozier, J., Bair, E. H. and Davis, R. E.: Estimating the spatial distribution of snow water equivalent in the world's mountains, WIREs Water., 3, 461–474, https://doi.org/10.1002/wat2.1140, 2016.

Estilow, T. W., Young, A. H. and Robinson, D. A.: A long-term Northern Hemisphere snow cover extent data record for climate studies and monitoring, Earth Syst. Sci. Data., 7, 137-142, https://doi.org/10.5194/essd-7-137-2015, 2015.

Fang, Y., Liu, Y. and Margulis, S. A.: A Western United States snow reanalysis datasets over the Landsat era from water years 1985 to 2021, Sci Data., 9, 677, https://doi.org/10.1038/s41597-022-01768-7, 2022.

Gao, Y., Lu, N., Dai, Y. and Yao, T.: Reversal in snow mass trends on the Tibetan Plateau and their climatic causes, J. Hydrol., 620, 129438, https://doi.org/10.1016/j.jhydrol.2023.129438, 2023.

González-Herrero, S.: A tall tower to measure the blowing snow in Antarctica, Nat. Rev. Earth Environ., 6, 229, https://doi.org/10.1038/s43017-025-00664-z, 2025.

Groisman, P. Y., Karl, T. R. and Knight, R. W.: Observed impact of snow cover on the heat balance and the rise of continental spring temperatures, Science., 263, 198–200, https://doi.org/10.1126/science.263.5144.198, 1994.

Hamlet, A. F., Mote, P. W., Clark, M. P. and Lettenmaier, D. P.: Effects of temperature and precipitation variability on snowpack trends in the western United States, J. Climate., 18, 4545-4561, https://doi.org/10.1175/JCLI3538.1, 2005.

Hou, M. Cuo, L., Murodov, A., Ding, J., Luo, Y., Liu, T., Chen X.: Streamflow composition and the contradicting impacts of anthropogenic activities and climate change on the streamflow in the Amu Darya Basin, Central Asia, J. Hydrometeorol., 24, 185–201, https://doi.org/10.1175/JHM-D-22-0040.1, 2023.

Hou, M., Cuo L., Xu H.: Hydrological response to twenty-first century climate change in the Amu Darya Basin, Central Asia, J. Hydrol. Reg. Stud., 61, 102606, https://doi.org/10.1016/j.ejrh.2025.102606, 2025.

https://doi.org/10.5194/egusphere-2025-4849
Preprint. Discussion started: 8 December 2025

Houle, E. S., Livneh, B. and Kasprzyk, J. R.: Exploring snow model parameter sensitivity using Sobol' variance decomposition, Environ. Model. Softw., 89, 144–158, https://doi.org/10.1016/j.envsoft.2016.11.024, 2017.

Immerzeel, W. W., Lutz, A. F., Andrade, M., Bahl, A., Biemans, H., Bolch, T., Hyde, S., Brumby, S., Davies, B. J., Elmore, A. C., Emmer, A., Feng, M., Fernández, A., Haritashya, U., Kargel, J. S., Koppes, M., Kraaijenbrink, P. D. A., Kulkarni, A. V., Mayewski, P. A., Nepal, S., Pacheco, P., Painter, T. H., Pellicciotti, F., Rajaram, H., Rupper, S., Sinisalo, A., Shrestha, A. B., Viviroli, D., Wada, Y., Xiao, C., Yao, T., Baillie, J. E. M.: Importance and vulnerability of the world's water towers, Nature., 577, 364-369, https://doi.org/10.1038/s41586-019-1822-y, 2020.

Israeli, O.: A Shapley-based decomposition of the R-Square of a linear regression, J. Econ. Inequal., 5, 199–212, https://doi.org/10.1007/s10888-006-9036-6, 2007.

Jin H., Chen X., Zhong R., Wu P., Ju Q., Zeng J., Yao T.: Extraction of snow melting duration and its spatiotemporal variations in the Tibetan Plateau based on MODIS product, Adv. Space Res., 70., 15-34, https://doi.org/10.1016/j.asr.2022.04.018, 2022.

King, J. C., Anderson, P. S. and Mann, G. W.: The seasonal cycle of sublimation at Halley, Antarctica, J. Glaciol., 47, 156–160, https://doi.org/10.3189/172756501781832548, 2001.

Kiranyaz, S., Avci, O., Abdeljaber, O., Ince, T., Gabbouj, M., Inman D. J.: 1D convolutional neural networks and applications: A survey, Mech. Syst. Signal Process., 151, 107398, https://doi.org/10.1016/j.ymssp.2020.107398, 2021.

Kirkham, J. D., Koch, I., Saloranta, T. M., Litt, M., Stigter, E. E., Møen, K., Thapa, A., Melvold, K., Immerzeel, W. W.: Near real-time measurement of snow water equivalent in the Nepal Himalayas, Front. Earth Sci., 7, 177, https://doi.org/10.3389/feart.2019.00177, 2019.

Kochendorfer, J., Earle, M., Rasmussen, R., Smith, C., Yang, D., Morin, S., Mekis, E., Buisan, S., Roulet, Y., Landolt, S., Wolff, M., Hoover, J., Thériault, J. M., Lee, G., Baker, B., Nitu, R., Lanza, L., Colli, M., Meyers, T.: How well are we measuring snow post-SPICE? Bull. Am. Meteorol. Soc., 103, E370-E388, https://doi.org/10.1175/BAMS-D-20-0228.1, 2022.

https://doi.org/10.5194/egusphere-2025-4849
Preprint. Discussion started: 8 December 2025

Körner, C., Paulsen, J. and Spehn, E. M.: A definition of mountains and their bioclimatic belts for global comparisons of biodiversity data, Alp. Bot., 121, 73–78, https://doi.org/10.1007/s00035-011-0094-4, 2011.

Kraaijenbrink, P. D. A., Stigter, E. E., Yao, T. and Immerzeel, W. W.: Climate change decisive for Asia's snow meltwater supply, Nat. Clim. Change., 11, 591–597, https://doi.org/10.1038/s41558-021-01074-x, 2021.

Li, H., Wang, J., Bai, Y., Li, Z. and Dou, Y.: The snow hydrological processes during a representative snow cover period in Binggou watershed in the Upper Reaches of Heihe River, J. Glaciol. Geocryol., 31, 293-300, 2009.

Li, H., Wang, J. and Hao, X.: Influence of blowing snow on snow mass and energy exchanges in the Qilian mountains, J. Glaciol. Geocryol., 34, 1084-1090, https://doi.org/10.7522/j.issn.1000-0240.2012.0132, 2012.

Li, H., Zhang, Y., Li, X., Yang, D. and Hao, X.: Tracing snowmelt paths in an integrated hydrological model for understanding seasonal snowmelt contribution at basin scale, J. Geophys. Res. Atmos., 124, 8874–8895, https://doi.org/10.1029/2019JD030760, 2019.

Li, N., Cuo, L. and Zhang, Y.: On the freeze-thaw cycles of shallow soil and connections with environmental factors over the Tibetan Plateau, Clim. Dyn., 57, 3183–3206, https://doi.org/10.1007/s00382-021-05860-3, 2021.

Li, N., Cuo, L. and Zhang, Y.: The synthesis of potential factors contributing to the asynchronous warming between air and shallow ground since the 2000s on the Tibetan Plateau, Geoderma., 441, 116753, https://doi.org/10.1016/j.geoderma.2023.116753, 2024.

Li, W., Guo, W., Qiu, B., Xue, Y., Hsu, P. C., Wei, J.: Influence of Tibetan Plateau snow cover on East Asian atmospheric circulation at medium-range time scales, Nat. Commun., 9, 4243, https://doi.org/10.1038/s41467-018-06762-5, 2018.

Li, Y., Pan, J., Xiong, C., Jiang, L. and Shi, J.: Snow depth and snow cover over the Tibetan Plateau observed from space in against ERA5: Matters of scale, Clim. Dyn., 60, 1523-1541, https://doi.org/10.1007/s00382-022-06376-0, 2023.

https://doi.org/10.5194/egusphere-2025-4849
Preprint. Discussion started: 8 December 2025

Liang, X., Lettenmaier D. P., Wood E. F., and Burges S. J.: A simple hydrologically based model of land surface water and energy fluxes for general circulation models, J. Geophys. Res., 99, 14 415–14 428, https://doi.org/10.1029/94JD00483, 1994.

Liang, X., Wood, E. F. and Lettenmaier, D. P.: Surface soil moisture parameterization of the VIC-2L model: Evaluation and modification, Glob. Planet. Change., 13, 195–206, https://doi.org/10.1016/0921-8181(95)00046-1, 1996.

Liston, G. E. Haehnel, R. B., Sturm, M., Hiemstra, C. A., Berezovskaya, S., Tabler. R. D.: Simulating complex snow distributions in windy environments using SnowTran-3D, J. Glaciol., 53, 241–256, https://doi.org/10.3189/172756507782202865, 2007.

Liu, J., Yang, Z. L., Jia, B., Wang, L., Wang, P., Xie, Z., Shi, C.: Elucidating dominant factors affecting land surface hydrological simulations of the Community Land Model over China, Adv. Atmos. Sci., 40, 235–250, https://doi.org/10.1007/s00376-022-2091-5, 2023a.

Liu, Z., Cuo, L. and Sun, N.: Tracking snowmelt during hydrological surface processes using a distributed hydrological model in a mesoscale basin on the Tibetan Plateau, J. Hydrol., 616, 128796, https://doi.org/10.1016/j.jhydrol.2022.128796, 2023b.

Lundquist, J. D., Vano, J., Gutmann, E., Hogan, D., Schwat, E., Haugeneder, M., Mateo, E., Oncley, S., Roden, C., Osenga, E., Carver, L.: Sublimation of snow, Bull. Am. Meteorol. Soc., 105, E975–E990, https://doi.org/10.1175/BAMS-D-23-0191.1, 2024.

Ma, L. and Qin, D.: Spatial-temporal characteristics of observed key parameters for snow cover in China during 1957–2009, J. Glaciol. Geocryol., 34, 1–11, https://doi.org/10.7522/j.issn.1000-0240.2012.0001, 2012.

Ma, Q., Keyimu M., Li X., Wu S., Zeng F., Lin L.: Climate and elevation control snow depth and snow phenology on the Tibetan Plateau, J. Hydrol., 617, 128938, https://doi.org/10.1016/j.jhydrol.2022.128938, 2023.

Miao, C., Immerzeel, W.W., Xu, B., Yang, K., Duan, Q., Li, X.: Understanding the Asian water tower requires a redesigned precipitation observation strategy, Proc. Natl. Acad. Sci. U.S.A., 121, e2403557121, https://doi.org/10.1073/pnas.2403557121, 2024.

https://doi.org/10.5194/egusphere-2025-4849
Preprint. Discussion started: 8 December 2025

Mokhtar, A., Jalali, M., He, H., Al-Ansari, N., Elbeltagi, A., Alsafadi, K., Abdo, H. G., Sammen, S. S., Gyasi-Agyei, Y., Rodrigo-Comino J.: Estimation of SPEI Meteorological Drought Using Machine Learning Algorithms, IEEE Access., 9: 65503–65523, https://doi: 10.1109/ACCESS.2021.3074305, 2021.

Moriasi, D. N., Arnold, J. G., Van Liew, M. W., Bingner, R. L., Harmel, R. D., Veith, T. L.: Model evaluation guidelines for systematic quantification of accuracy in watershed simulations, Trans. ASABE., 50, 885–900, https://doi.org/10.13031/2013.23153, 2007.

Paix, M. J., Li, L. L., Ge, J., Dieu, H. J. and Teoneste, N.: Analysis of snowmelt model for flood forecast for water in arid zone: Case of Tarim River in Northwest China, Environ. Earth Sci., 66, 1423–1429, https://doi.org/10.1007/s12665-011-1353-9, 2012.

Pomeroy, J. W. and Gray, D. M.: Snowcover Accumulation, Relocation and Management, National Hydrology Research Institute, Canada, Saskatoon, Saskatchewan, ISBN 978-0660158167, 1995.

Pomeroy, J. W. and Li, L.: Prairie and arctic areal snow cover mass balance using a blowing snow model, J. Geophys. Res. Atmos., 105, 26619–26634, https://doi.org/10.1029/2000JD900149, 2000.

Poudel, A., Cuo, L., Gyawali, A. R. and Li, N.: Spatiotemporal Patterns of Hydrometeorological Extremes over 1986–2015 in Nepal, J. Hydrometeorol., 23, 573-596, https://doi.org/10.1175/JHM-D-21-0122.1, 2022.

Pu, Z. and Xu, L.: MODIS/Terra observed snow cover over the Tibetan Plateau: Distribution, variation and possible connection with the East Asian summer monsoon (EASM), Theor. Appl. Climatol., 97, 265–278, https://doi.org/10.1007/s00704-008-0074-9, 2009.

Pulliainen, J., Luojus, K., Derksen, C., Mudryk, L., Lemmetyinen, J., Salminen, M., Ikonen, J., Takala, M., Cohen, J., Smolander, T., Norberg, J.: Patterns and trends of Northern Hemisphere snow mass from 1980 to 2018, Nature., 581, 294–298, https://doi.org/10.1038/s41586-020-2258-0, 2020.

Qin, D., Liu, S. and Li, P.: Snow cover distribution, variability, and response to climate change in western China, J. Climate., 19, 1820–1833, https://doi.org/10.1175/JCLI3694.1, 2006.

https://doi.org/10.5194/egusphere-2025-4849
Preprint. Discussion started: 8 December 2025

Qin, Y., Hong, C., Zhao, H., Siebert, S., Abatzoglou, J. T., Huning, L. S., Sloat, L. L., Park, S., Li, S., Munroe, D. K., Zhu, T., Davis, S. J., Mueller, N. D.: Snowmelt risk telecouplings for irrigated agriculture, Nat. Clim. Change., 12, 1007–1015, https://doi.org/10.1038/s41558-022-01509-z, 2022.

Sahadeep, T.: Modeling the contribution of sublimation and snowmelt to snow depth dynamics in eastern Tibetan Plateau, thesis, M.S. thesis, University of Chinese Academy of Sciences, Beijing, China, 2019.

Saloranta, T., Thapa, A., Kirkham, J. D., Koch, I., Melvold, K., Stigter, E., Litt, M., Møen, K.: A model setup for mapping snow conditions in High-Mountain Himalaya, Front. Earth Sci., 7, 129, https://doi.org/10.3389/feart.2019.00129, 2019.

Schaake, J. C.: From Climate to Flow: Climate Change and US Water Resources, John Wiley, New York, 177-206, ISBN 978-0-471-61838-6,1990.

Screen, J. A. and Simmonds, I.: The central role of diminishing sea ice in recent Arctic temperature amplification, Nature., 464, 1334–1337, https://doi.org/10.1038/nature09051, 2010.

Shao, D., Li, H., Wang, J., Hao, X., Che, T., Ji, W.: Reconstruction of a daily gridded snow water equivalent product for the land region above 45°N based on a ridge regression machine learning approach, Earth Syst. Sci. Data., 14, 795–809, https://doi.org/10.5194/essd-14-795-2022, 2022.

Smith, T. and Bookhagen, B.: Changes in seasonal snow water equivalent distribution in High Mountain Asia (1987 to 2009), Sci. Adv., 4, e1701550, https://doi.org/10.1126/sciadv.170155, 2018.

Sobol', I. M.: Sensitivity estimates for nonlinear mathematical models and their Monte Carlo estimation, Math. Model. Comput. Exp., 1, 407–417, https://doi.org/10.1016/S0378-4754(00)00270-6, 1993.

StiGter, E. E., Litt, M., Steiner, J. F., Bonekamp, P. N. J., Shea, J. M., Bierkens, M. F. P., Immerzeel, W. W.: The importance of snow sublimation on a Himalayan glacier. Front. Earth Sci. 6, 108, https://doi.org/10.3389/feart.2018.00108, 2018.

Turner, A. G. and Slingo, J. M.: Using idealized snow forcing to test teleconnections with the Indian summer monsoon in the Hadley Centre GCM, Clim. Dyn., 36, 1717–1735, https://doi.org/10.1007/s00382-010-0805-3. 2011.

https://doi.org/10.5194/egusphere-2025-4849
Preprint. Discussion started: 8 December 2025

Ueno, K., Tanaka, K., Tsutsui, H. M. S. and Li, J.: Snow cover conditions in the Tibetan Plateau observed during the winter of 2003/2004, Arct. Antarct. Alp. Res., 39, 152–164, http://doi.org/10.1657/1523-0430(2007)39[152:SCCITT]2.0.CO;2., 2007.

Wang, C., Duan, Q., Gong, W., Ye, A., Di, Z., Miao, C.: An evaluation of adaptive surrogate modeling based optimization with two benchmark problems, Environ. Model. Softw., 60, 167-179, https://doi.org/10.1016/j.envsoft.2014.05.026, 2014.

Wang, L., Yao, T., Chai, C., Cuo, L., Su, F., Zhang, F., Yao, Z., Zhang, Y., Li, X., Qi, J., Hu, Z., Liu, J., Wang, Y.: TP-River: Monitoring and quantifying total river runoff from the Third Pole, Bull. Am. Meteorol. Soc., 102, E948–E965, https://doi.org/10.1175/BAMS-D-20-0207.1, 2021.

Wang, Z., Wu, R. and Huang, G.: Low-frequency snow change over the Tibetan Plateau, Int. J. Climatol., 38, 949–963, https://doi.org/ 10.1002/joc.5221, 2018.

Winkler, M., Schellander, H. and Gruber, S.: Snow water equivalent exclusively from snow depths and their temporal changes: The Δ SNOW model, Hydrol. Earth Syst. Sci., 25, 1165–1187, https://doi.org/10.5194/hess-25-1165-2021, 2021.

Wu, R. and Kirtman, B. P.: Observed relationship of spring and summer East Asian rainfall with winter and spring Eurasian snow, J. Clim., 20, 1285–1304, https://doi.org/10.1175/JCLI4068.1, 2007.

Yang, M., Nelson, F. E., Shiklomanov, N. I., Guo, D. and Wan, G.: Permafrost degradation and its environmental effects on the Tibetan Plateau: A review of recent research, Earth Sci. Rev., 103, 31–44, https://doi.org/10.1016/j.earscirev.2010.07.002, 2010.

Yang, T., Li, Q., Chen, X., Hamdi, R., Maeyer, P. D., Li, L. Variation of snow mass in a regional climate model downscaling simulation covering the Tianshan Mountains, Central Asia, J. Geophys. Res. Atmos., 126, e2020JD034183, https://doi.org/10.1029/2020JD034183, 2021.

Yang, Y., Chen, R., Liu, G., Liu, Z. and Wang, X.: Trends and variability in snowmelt in China under climate change, Hydrol. Earth Syst. Sci., 26, 305–329, https://doi.org/10.5194/hess-26-305-2022, 2022.

You Q., Kang S., Ren G., Fraedrich K., Pepin N., Yan Y., Ma L.: Observed changes in snow depth and number of snow days in the eastern and central Tibetan Plateau, Clim. Res., 46, 171-183, https://doi.org/10.3345/cr00985, 2011.

https://doi.org/10.5194/egusphere-2025-4849
Preprint. Discussion started: 8 December 2025

You, Y., Huang, C., Zhang, Y. and Hou, J.: Sensitivity evaluation of snow simulation to multi-parameterization schemes in the Noah-MP model, Adv. Earth Sci., 34, 356–365, https://doi.org/10.11867/j.issn.1001-8166.2019.04.0356, 2019.

Zhang, L., Su, F., Yang, D., Hao, Z. and Tong, K.: Discharge regime and simulation for the upstream of major rivers over Tibetan Plateau, J. Geophys. Res. Atmos., 118, 8500-8518, https://doi.org/10.1002/jgrd.50665, 2013.

Zhang, R., Zhang, R., Zuo, Z. and Li, W.: Temporal and spatial features and inter-annual variability of wintertime snow mass balance over China, Int. J. Climatol., 36, 3897–3907, https://doi.org/10.1002/joc.4599, 2015.

Zheng, Q., Chen, R., Han, C. and Song, Y.: Intercomparison study on precipitation observations of TRwS204 and Chinese standard precipitation gauge in the Qilian Mountains, Plateau Meteorol., 37, 747–756, 2018.

Zhou, B., Wang, Z., Shi, Y., Xu, Y. and Han, Z.: Historical and future changes of snowfall events in China under a warming background, J. Clim., 31, 5873–5899, https://doi.org/10.1175/JCLI-D-17-0428.1, 2018.

Zhou, J., Pomeroy, J. W., Zhang, W., Cheng, G., Wang, G., Chen C.: Simulating cold regions hydrological processes using a modular model in the west of China, J. Hydrol., 509, 13-24, https://doi.org/10.1016/j.jhydrol.2013.11.013, 2014.

Zhu, F., Li, X., Qin, J., Yang, K., Cuo, L., Tang, W.: Integration of multisource data to estimate downward longwave radiation based on deep neural networks, IEEE Trans, Geosci. Remote Sens., 60, 1-15, https://doi.org/10.1109/TGRS.2021.3094321, 2022.